NON-CLINICAL USES OF THE GAMMA KNIFE PERFEXION: SMALL ANIMAL IRRADIATION AND CONVOLUTION ALGORITHM EVALUATION

A Dissertation

presented to

the Faculty of the Graduate School

at the University of Missouri

In Partial Fulfillment

of the Requirements for the Degree

Doctor of Philosophy

---

by JEREMY CATES

Dr. Robert Drzymala, Advisor
Dr. Sudarshan Loyalka, Advisor

December 2017

The undersigned, appointed by the dean of the Graduate School, have examined the dissertation entitled

NON-CLINICAL USES OF THE GAMMA KNIFE PERFEXION: SMALL ANIMAL IRRADIATION AND CONVOLUTION ALGORITHM EVALUATION

presented by Jeremy Cates,

a candidate for the degree Doctor of Philosophy,

and hereby certify that, in their opinion, it is worthy of acceptance.

Dr. Sudarshan Loyalka

Dr. Tushar Ghosh

Dr. Lixin Ma

Dr. Mark Prelas

Dr. Robert Tompson

ACKNOWLEDGEMENTS

I would like to thank the faculty and staff at the Nuclear Science and Engineering Institute at the University of Missouri. The faculty at NSEI are exceptional, and the quality of classes I were able to attend was outstanding.

I would also like to thank the faculty and staff in the Radiation Oncology Department at Washington University in St. Louis. I appreciate being able to learn from and perform research with the many medical physicists in the department, which is one of the leading Medical Physics departments in the country. In addition, I extend my thanks to the Gamma Knife radiosurgery team of nurses who were of great help in facilitating my research work on the department's Gamma Knife machine.

I would like to specifically thank Dr. Sudarshan Loyalka at NSEI, and Dr. Robert Drzymala and Dr. Joel Garbow at WUSTL for their significant contribution to the research and publication work that I was able to do.

Finally, I would like to thank my wife, Jill Sutter, for her support and patience during my graduate school career.

TABLE OF CONTENTS

LIST OF FIGURES AND TABLES

ABSTRACT

Purpose: The purpose of this project was two-fold. One, to test the accuracy and usefulness of a clinically unused dose calculation algorithm for the Leksell Gamma Knife Perfexion radiosurgery unit that accounts for heterogeneities in the patient volume. This process included designing, fabricating, and testing a novel phantom from idea stage through production and use. Two, to facilitate and provide dosimetry for irradiating a large number of mice and rats to develop a murine model of radiation induced necrosis in the brain.

Methods/Materials: To test the dose calculation algorithm, we used a commercially available anthropomorphic head phantom and EBT2 radiochromic film to evaluate predicted vs measured dose delivery for the clinically accepted algorithm, which assumes a homogeneous treatment volume, and the convolution algorithm, which takes into account heterogeneities within the treatment volume. In addition, we designed and fabricated a novel phantom that could accommodate various heterogeneities along with EBT2 film and an ion chamber. We again evaluated predicted vs measured dose with varying material configurations for both algorithms. To assist the murine necrosis model, we developed a novel mouse positioning and irradiation system utilizing the Gamma Knife Perfexion that was designed to be accurate, repeatable and efficient. We designed an animal immobilizing planform that could be incorporated into the clinical protocol for acquiring patient image data, image registration, and treatment planning.

Results: We demonstrated that the convolution algorithm is accurate to within a clinically acceptable three percent in cases of extreme heterogeneities, and it is clinically significantly more accurate than the standard homogeneous algorithm when large heterogeneities are present in the treatment volume. In addition, we were able to facilitate the development of a robust murine radiation necrosis model by irradiating more than 1,000 mice to a spatial accuracy of within 0.5 millimeters in all directions and to within five percent accuracy of prescription dose.

Conclusion: During the course of this work we successfully completed two large undertakings that are representative of tasks often asked of a clinical medical physicist. First, to evaluate a treatment delivery option in the radiation oncology clinic and make evidence based recommendations for clinical protocols. And second, to provide a reliable and scientifically sound service to collaborators and outside research groups when physics expertise is required.

Chapter 1
Introduction

1.1 Motivation

Preclinical in-vivo experiments using small animals have become a necessity to facilitate progress from in-vitro cell experiments to clinical implementation of effective therapeutic procedures. This is especially true in translational cancer research, which can include radiotherapy, chemotherapy, and radio-sensitizing and/or radio-protecting compounds. These preclinical experiments are designed to discover the fundamental characteristics of cancer, including tumor formation and growth, metastasis of disease, and physiological effects including angiogenesis and hypoxia. Small animal experiments facilitate the development and optimization of treatment options provided by radiation oncology. Mice and rats are most commonly used for preclinical in-vivo studies due to their small size, ease of handling, low cost, consistent growth characteristics, and rapid reproduction rate.

Mice and rats were traditionally irradiated using large stationary fields and unchanging standard collimation without imaging. Over time, human radiation therapy has evolved to include three-dimensional inverse treatment planning along with image-guided, conformal, and extremely accurate beam geometries. As these improved treatment practices became more widespread, the use of clinical radiotherapy treatment devices for small-animal experiments followed, which could incorporate image guidance and smaller, more conformal fields. Additionally, dedicated small-animal irradiators were developed at research institutions and became available commercially. These dedicated machines were appealing to researchers due to their relative lower cost and reduced need

for large, heavily shielded rooms. However, acquiring dedicated small-animal irradiation machines required either funding specifically for a small-animal research or a heavy investment of extensive physics and engineering manpower.

A research group at our institution was interested in irradiating a very large number of mice with a very small treatment volume in order to develop a novel murine model of radiation necrosis. It was determined that the Gamma Knife Perfexion, a clinically used stereotactic radiosurgery unit, could be used for this purpose. As there is no commercially available small-animal attachment available for the Perfexion, it was undertaken to develop an irradiation system suitable for this research.

The Gamma Knife Perfexion (Elekta Corporation) is a commercial stereotactic radiosurgery unit used in many radiation oncology clinics around the world to treat more than 20,000 patients each year. The Gamma Knife is a specialty machine designed for the treatment of tumors and vascular malformations within the head. It is able to deliver highly conformal doses to volumes as small as three cubic-centimeters with rapid dose falloff. This volume is small enough to be able to irradiate a single hemisphere of a mouse brain. Additionally, the positioning accuracy of the Perfexion is advertised to be within 0.2 millimeters. These capabilities made the Gamma Knife Perfexion a promising option for this research.

Due to its use mainly related to the human head, the Perfexion's dose calculation algorithm accepted and used clinically is a homogeneous algorithm, meaning is treats the entire treatment volume as a unit density, water equivalent substance. This is accepted clinical practice and has been since the beginning of the machine's use. However, in a recent release of the treatment planning software Leksell GammaPlan, a convolution-

based algorithm that takes heterogeneities within the contoured volume into account was included. This algorithm is not yet used clinically and may not offer any outcome benefit if it were to be used. When asked why the algorithm was included at all, a representative of the company responded that it was included as an additional tool in a physicist's toolbox, to be used at their discretion, but not endorsed or recommended by the company.

1.2 Objectives and Scope

To facilitate the irradiation of a large number of mice for the necrosis research, we wanted to devise a system to make the animal irradiation process fast, accurate, and easily repeatable. We decided to construct a novel mouse holder platform that could function as a way to position the animals for both imaging and irradiation. The platform would therefore need to be able to attach to a CT couch as well as to the Gamma Knife stereotactic system. It would also have to be user-friendly enough that the mice could be positioned such that the head could be aligned with sub-millimeter accuracy for every imaging session and irradiation session. This would allow one set of images to be used for multiple irradiation sessions, even if different technicians handled the animals for different sessions. Finally, we needed to be able to test the dosimetric accuracy of the planned treatments, therefore representative phantoms were constructed to allow for radiochromic film dosimetry. The scope of the project was to be able to treat cohorts of mice from week to week, with each irradiation sessions lasting only a few hours, indefinitely. We wanted the system to have sub-millimeter accuracy throughout the duration of the experiment, and the delivered dose accuracy needed to be within 10% of predicted dose.

We have also undertaken testing of the convolution algorithm to determine a) its dose calculation accuracy, and b) its potential use at a clinical and/or research tool. We have done this by utilizing a commercially available anthropomorphic head phantom coupled with EBT2 film as well as by developing a novel, in-house heterogeneous phantom that incorporates both EBT 2 film and an ion chamber. Fabrication of the novel phantom would have to be within the price range of commercially available phantoms to make the project cost effective, and it would need to enable clinically relevant research that provided data robust enough to make clinical decisions, namely whether to use the Convolution algorithm instead of the current TMR 10 algorithm, and if so in what cases.

1.3 Organization of the Thesis

The thesis is organized as follows:

Chapter 1 is an introduction to and justification for the project, including the scope of what we wanted to accomplish.

Chapter 2 is a description of the Gamma Knife Perfexion, a brief description of its clinical procedures, and an in-depth discussion of the dose calculation algorithms.

Chapter 3 describes an experiment that compares the planned and delivered dose to an anthropomorphic head phantom containing radiochromic film. The dose distributions are planned using both the TMR 10 and Convolution algorithms, and dosimetric accuracy for each is reported.

Chapter 4 describes the development and fabrication of a novel phantom utilized to test the capabilities of the Convolution algorithm to accurately account for heterogeneities within a treatment volume.

Chapter 5 describes the development of a novel mouse holding platform used to irradiate a large number of mice. It also describes the special and dosimetric accuracy of the irradiation system, as well as the outcomes of the mouse research reached by using the Gamma Knife and our irradiation system.

Chapter 6 offers a discussion of and conclusion to the entire thesis project.

Chapter 2
The Gamma Knife

2.1 The Gamma Knife Perfexion

In 1951, Lars Leksell introduced the concept of radiosurgery to the medical community. He developed a technique that utilized a large number of converging beams of ionizing radiation to induce a small volume of necrosis in the target area. His first fixed-source Cobolt-60 unit was named Gamma Knife. Gamma Knife surgery gained acceptance in the 1980s, helped along by the increased use of MRI imaging to improve the safety and efficacy of radiosurgery. The most current and advanced iteration of his machine is the Gamma Knife Perfexion. The world's first Perfexion unit became operational at Timone University Hospital of Marseille on July 10, 2016.

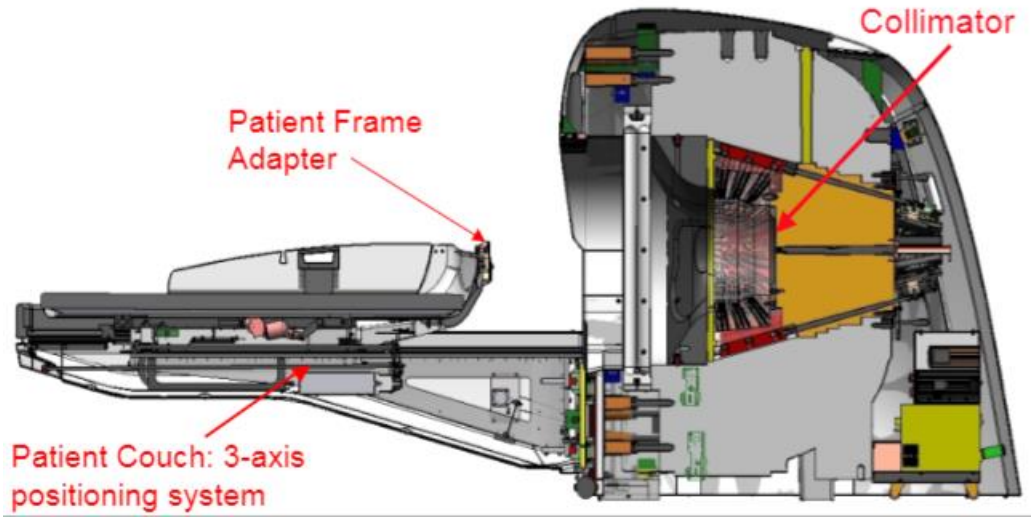

Fig 2.1: Gamma Knife Perfexion schematic

The Gamma Knife Perfexion is a radiosurgical treatment device that uses 192 high-activity Cobalt-60 sources arranged symmetrically around an isocenter. Cobolt-60

releases gamma radiation of two primary energies, 1.17 MeV and 1.33 MeV, and the two most probable photon interactions are photoelectric absorption and Compton scattering. Compton scattering is the main mode of radiation interaction in human anatomy. The gamma rays interact within a material to scatter through lower energies. Tungsten collimators are arranged into eight sectors of 24 sources each. Each sector can be set to collimator sizes of either four, eight, or sixteen millimeter diameter spheres at the focus, or isocenter. The sectors may be set at different collimator sizes at the same time, but each of the 24 individual sources within a given sector are all restricted to the same collimator size. Additionally, any number of sectors may be blocked while other sectors are open, but again, all sources within an individual sector will be set to the same setting. The beam off position significantly improves flexibility in treatment planning because it increases the number of possible beam arrangements when avoiding critical structures is difficult. Also, being able to turn off all beams during treatment allows the couch to move to a new position when treating a patient with multiple tumors, saving significant time. The patient is immobilized from the neck up by utilizing a cranial frame attached to the skull which is then positioned on the treatment couch. The patient is imaged with this same frame for treatment planning, which allows the coordinate system of the machine to be registered to the patient's image data. This is what facilitates the Perfexion's high degree of positioning accuracy.

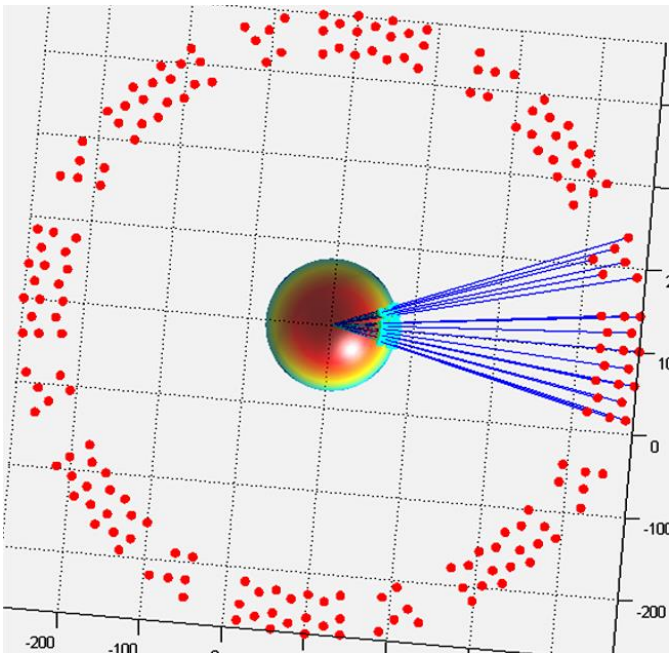

Fig 2.2 Schematic of 192 sources around isocenter, with one sector delivering 24 beams

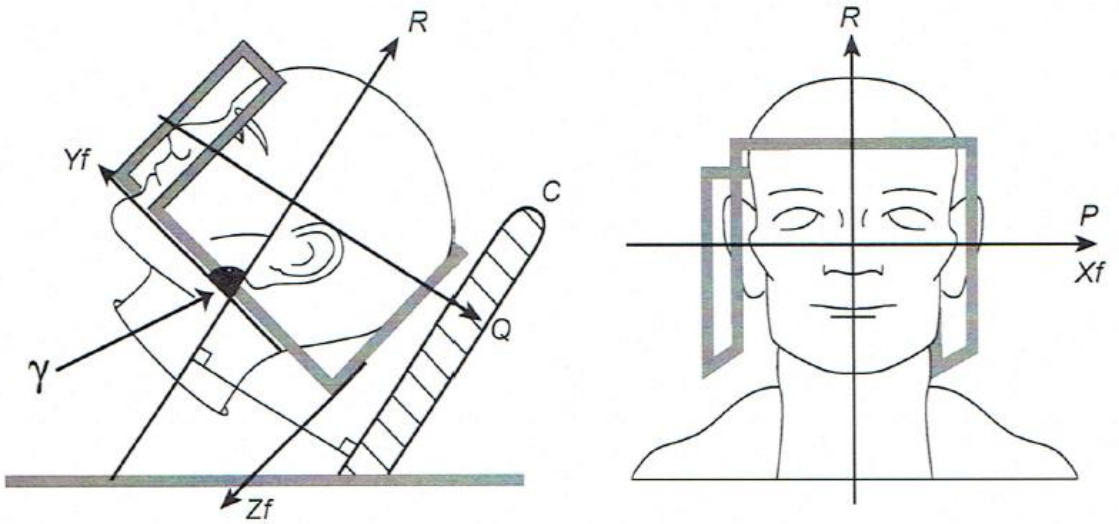

Fig. 2.3 Schematic of the Gamma Knife coordinate system and head frame

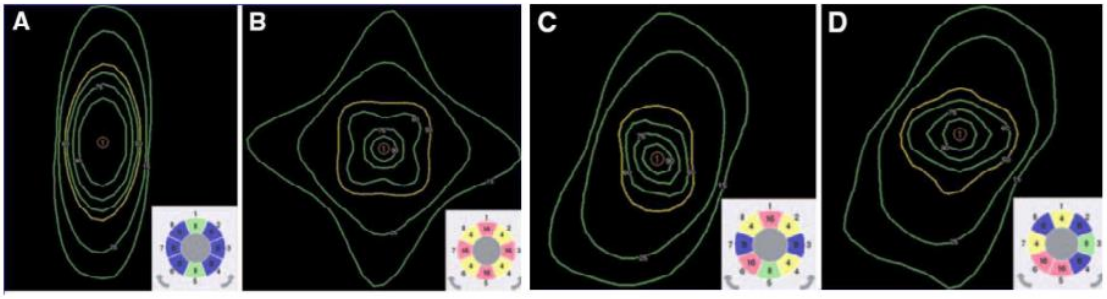

Fig. 2.4 Accurate representation of dose distribution from varying collimator arrangements

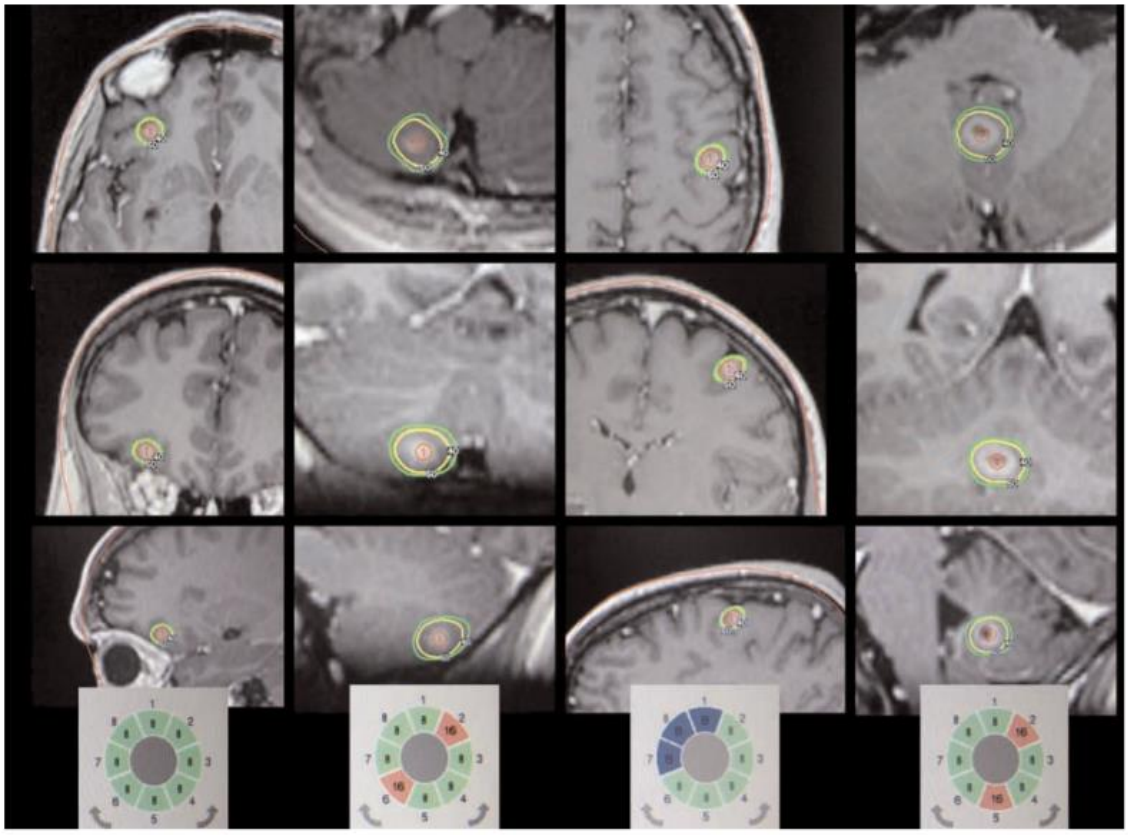

Fig. 2.5 Isodose lines of shots achieved with varying sector arrangements on patient CT images

Each iteration of the machine has made changes to the beam arrangement and collimator geometry, but by continuing to use multiple fixed converging beams as its central design allows practitioners to utilize the very large and prolonged worldwide

clinical experience gained to date, as well as thousands of peer-reviewed papers published to date.

Treatment planning is done on the manufacturer's Gamma Knife specific software utilizing image datasets from CT, MRI, and manual measurements. The entire radiosurgery treatment procedure is automated, which greatly alleviates staff workload, and the Gamma Knife primarily functions as its own "mini-clinic" within the radiation oncology department, allowing staff to become highly specialized and proficient. The current clinically accepted dose calculation algorithm used in the treatment planning system is the TMR 10 algorithm. Patient treatments utilize several nurses, a neurosurgeon, a radiation oncologist, and a medical physicist, making the quite resource intensive, which in turn means a highly efficient treatment system is essential.

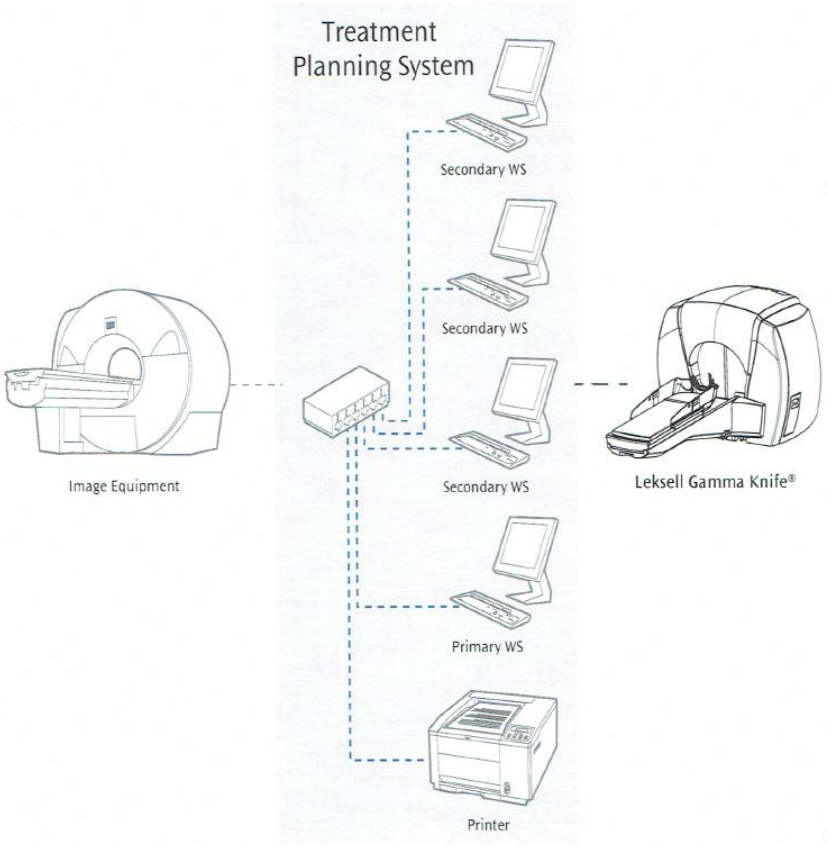

Fig. 2.6 Schematic of the Treatment Planning System Architecture

2.2. Gamma Knife Perfexion Dose Calculation Algorithms

For earlier versions of the Gamma Knife (Gamma Knife, B, C, 4, and 4C) the dose delivered from each separate cobalt-60 source was assumed to be identical. This means that the contribution to the total dose rate at the center of an 80mm spherical water phantom was assumed to be equal for all of the sources. Thus, it was possible to base calculations on measurements obtained from a single source channel and superimpose the dose from all other sources.

For the Gamma Knife Perfexion, the dose at a point is a linear superposition of the dose form all the sources. Due to the more complex geometry of the Perfexion, the dose from a single source at a nominated point will be dependent on the location of the source. Sources placed in the same ring are assumed to be identical, i.e. their contribution to the dose rate at the center of an 80mm spherical water phantom is equal. Sources placed in different rings are not identical since they give different contribution to the dose rate at the center of the phantom. Thus, a more complicated model is required to describe the dose deposition from each source.

The current clinically accepted calculation algorithm is the TMR 10 algorithm, and an additional Convolution algorithm is included in the treatment planning software. The TMR (Tissue Maximum Ratio) algorithm is based on the assumption that the tissue in the head from a dosimetrical point of view can be approximated with water. This assumption is not made with the Convolution algorithm. Convolution is a commonly used algorithm for dose calculation in radiation therapy. The primary difference between the convolution algorithm and the TMR algorithm is that the convolution algorithm takes

tissue heterogeneities in the patient into account and can model dose build-up effects near tissue boundaries.

2.2.1 TMR 10 Dose Calculation Algorithm

To model the dose for the TMR 10 algorithm, each type of collimator has been attached to a single source channel and the dose distribution has been measured. The measurements have been made at a focal distance that is specific for the collimator. For each collimator size there are five rings and the focal distances are different for each of the rings. In the experimental set-up, the beams have been attenuated in an 80mm spherical water phantom where radio-sensitive films are placed measuring the profile in a plane perpendicular to the beam. The 4mm collimators have the sources oriented along the symmetry axes of the collimators and the profiles are therefore radial. Because of the asymmetric orientation of the source compared to the symmetry axis of the 8mm and 16mm collimators, the profiles lack rotational symmetry and are therefore stored as two-dimensional profiles.

The dose calculation algorithm is based on some fundamental building blocks. Those are inverse square law, exponential attenuation in water, output factors and dose profiles.

The inverse square law is a consequence of the divergence of the photon flux of the beam. The number of photons passing a unit are of the beam will decrease as $1/r^2$ where r is the distance to the source.

The exponential attenuation expresses the fact that the photon flux decreases exponentially along the beam due to the interaction of photons with matter, implying that the energy deposited, i.e. the dose, decreases exponentially along the beam.

To mathematically describe the attenuation along the beam, the virtual source focus distance and the linear virtual attenuation co-efficient are introduced. These parameters are determined by a least square fitting of Monte Carlo generated profiles to the calculation model. The photon fluence field from the cobalt-60 sources is shaped in a unique way by the collimators leading to differences in dosimetric characteristics when the energy is deposited in the head of the patient. Therefore, the values of the parameters in the inverse square law and exponential attenuation will be collimator size and ring specific.

The lateral spread of dose is described by the dose profile. The alignment of the 4mm sources are with the collimator channels, while for the 8mm and 16mm collimators the sources are tilted compared to the collimator axis and the tilt angle depends on in which ring the source is located. The lack of rotational symmetry leads to the asymmetric profiles as described previously, and the dose profiles are planes rather than profiles. The profiles are scaled with the depth with a single parameter denoted the scaling distance. The scaling distance, being closely correlated (but not equal) to the source focus distance, is determined by Monte Carlo simulations.

The narrower the photon beams, the smaller the deposited dose. This dependency on the field size and the dose deposition is described by output factors. The output factors are dimensionless and normalized to the largest collimator sizes. Thus every output factor is less than or equal to one.

In TMR 10, the dose rate is attenuated by two terms with different attenuation coefficients; for the first term the distance from the skull surface is multiplied with μ_0, which is the linear attenuation coefficient for the photon fluence along the beam, and for the second term the distance from the focus point multiplied with the virtual attenuation coefficient for the particular beam. This formulation gives a good description of the dosimetry for shots placed far from the center of the head.

Equation 2.1 TMR 10 Dose Calculation Algorithm

$$D_i = \dot{D}_i t$$

$$\dot{D}_i = (\dot{D}_{center}\, \omega_{TMR10}^{c,r}\, ((d_{TMR10,\, vsf}^{c,r}) / (d_{TMR10,\, vsf}^{c,r} - dz))^2 \exp(\mu_{TMR10}^{c,r}\, dz) \exp(\mu_0\, (80 - d_{fei})\, P_{TMR10}^{c,r}(d, \vartheta)) \quad / \quad \Sigma\, n_r\, \omega_{TMR10}^{c=16,\, r}$$

$\dot{D}_i$	The dose rate at the point (X_{ip}, Y_{ip}, Z_{ip}) from the source *i*
T	Irradiation Time
$\dot{D}_{center}$	The dose rate is measured at the center of an 80mm spherical water phantom with all of the sectors having the 16mm collimator. It includes the exponential attenuation in time due to the decay of the source
$\omega_{TMR10}^{c,r}$	The output factor for the specific collimator size and ring, it is normalized to the 16mm collimator in the second ring
$d_{TMR10,\, vsf}^{c,r}$	The virtual source focus distance for the specific collimator size and ring
dz	The distance along the beam axis from the point of focus to the intersection with the line that is perpendicular to the beam axis and connects to the point.
μ_0	The linear attenuation coefficient for primary cobalt energies
$\mu_{TMR10}^{c,r}$	The linear virtual attenuation coefficient specific for each collimator size and ring
d_{fei}	Distance of the focus point from the skull entry point of the beam
$P_{TMR10}^{c,r}(d,\vartheta)$	Transverse dose profile; *d* is the distance from the focus, ϑ is the angle between the direction of the line extending from the source to the point *P* and the axis perpendicular to the beam for which ϑ=0
n_r	Number of sources in the ring

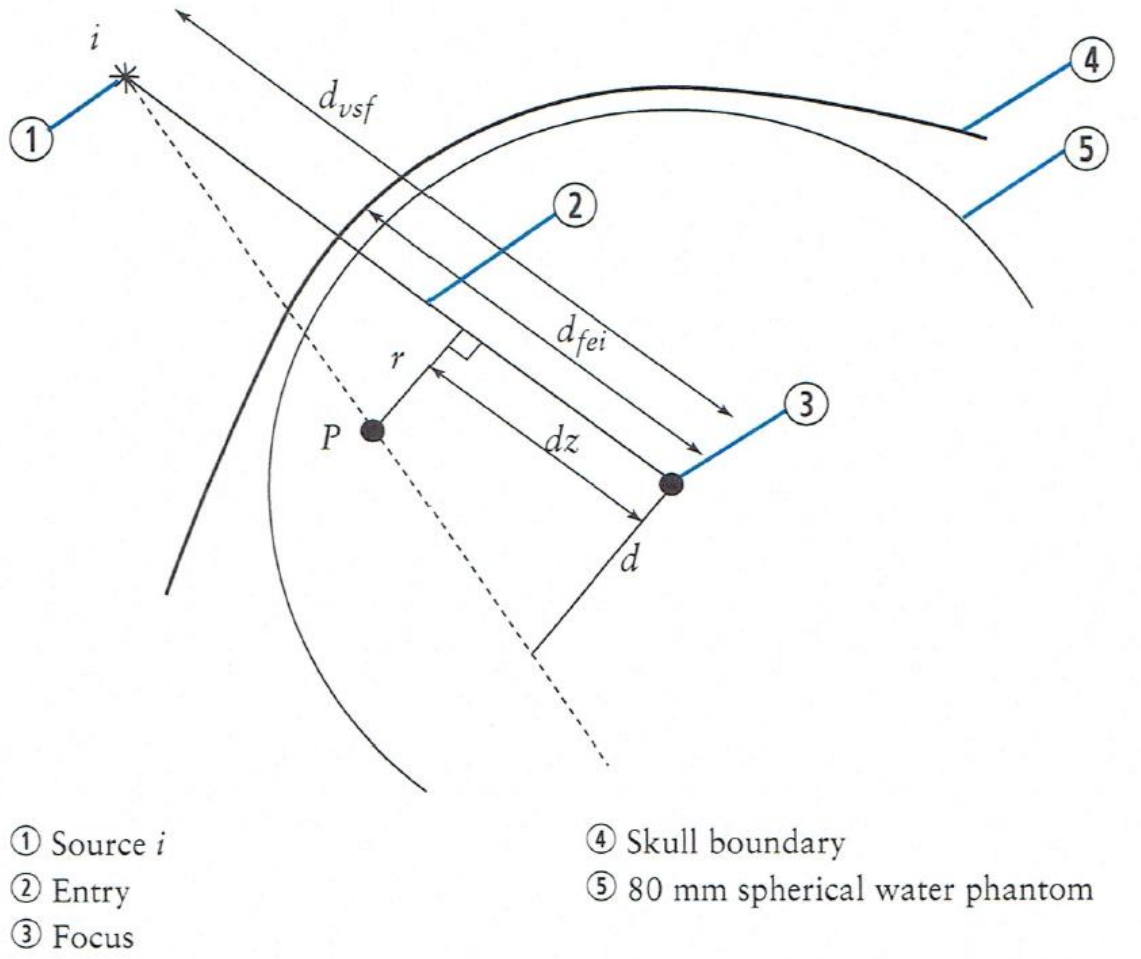

Fig 2.7 Geometry of beam in skull for TMR10 algorithm

2.2.2 Convolution Algorithm

While it is generally accepted that for treatments to the head and brain heterogeneities may be ignored during dose calculations, interfaces of disparate materials can create perturbations to the beam. Examples of those interfaces in the head include bone-tissue, bone-air, and tissue-air. The absence of electronic equilibrium near bone-tissue or air-tissue heterogeneities can cause dose calculation errors in treatment planning algorithms that assume homogeneous treatment volumes, like the TMR 10 algorithm. The dose falloff near air-tissue interfaces, caused by secondary electron disequilibrium,

can lead to overestimation of the dose at up to four millimeters from the interface. Additionally, dose delivered downstream of an air-tissue interface may be underestimated by up to seven percent due to overestimation of the photon beam attenuation in the air cavity. ()

Convolution is a commonly used algorithm for dose calculation in radiation therapy. The algorithm convolves a field describing the total amount of energy released by primary photons per unit mass (TERMA) with kernels describing how this energy is distributed by secondary particles. The development of the convolution algorithm was driven by several objectives, including a more reliable way to define the skull shape, a more accurate method for scattered dose calculation, and an improvement of the tissue inhomogeneity dose correction. More than ninety percent of the primary dose comes from the first scattered Compton electrons. This dose is very dependent on the sharp gradients of the primary fluence. Dose distribution further from the beam is dominated by scattered photons and lacks a sharp gradient. Taking this into consideration, the dose calculation is separated into two parts – calculation of dose due to scattering of primary photons (primary dose) and calculations of dose from scattered photons (scattered dose). The primary dose algorithm has a higher resolution and is more exact and therefore more computationally intense than scattered dose calculations.

2.2.2.1 TERMA Calculation

The energy fluence, i.e. flow of energy per unit area, is calculated by scaling reference fluence plane dose to geometric factors and material heterogeneities. The reference fluence plane is calculated at the center of a water phantom with radius 80mm using Monte Carlo simulations in a virtual model of the Leksell Gamma Knife Perfexion.

The energy fluence profiles for the 8 and 16mm collimators lack rotational symmetry therefore the profiles are stored in polar coordinates along 40 directions around the beam axis.

The energy released per unit volume is the linear attenuation coefficient times the energy fluence. The linear attenuation coefficient is proportional to the electron density at the energy release point.

Due to the divergent nature of the beams, the reference fluence is scaled with a geometrical factor depending on depth, and the fluence is scaled with the inverse square law. The reference fluence is scaled by an exponential attenuation along the beam. The attenuation coefficient is scaled with the radiological path length of the beam. The path length is calculated by ray tracing a fan of rays for the beam and is stored in a table. The ray tracing samples the electron densities in steps of 1mm and the spacing between the rays is 3mm at the focus.

To calculate the TERMA the expression for the energy released per volume unit is divided by the relative mass density to water. The TERMA is set to zero outside an off-axis threshold that depends on the collimator size. The TERMA is normalized such that the central value is 1 at the center of an 80mm water phantom.

The relative (to water) electron densities are defined by a user defined calibration curve and a CT definition. The relative (to water) mass densities are calculated form the electron densities by a bi-linear model that is fitted to biological materials.

2.2.2.2 Primary Dose

The primary dose is calculated by convolution of an energy deposition kernel with the TERMA. The kernel is pre-calculated by a Monte Carlo simulation forcing primary

photons to interact at a point and tracing the scattered electron in a homogeneous water material. The kernel describes the energy distribution from charged particles set in motion by primary photons interacting at a point. Alternatively, it describes the amount of energy received at a point from photon interaction in the surroundings of that point. The latter is used in this algorithm.

The following assumption were made:

- The electrons travel in straight lines between the interaction point and the dose deposition point.

- The radiological path lengths are assumed to be proportional to the average electron density between the interaction point and the dose deposition point. The radiological lengths are calculated with ray tracing where the electron densities are sampled in steps of 0.5mm.

- The kernel is discretized in spherical coordinates in 8 polar angles around the beam axis and 7 azimuthal angles.

- The value of the linear attenuation for the TERMA at the dose calculation point is used for all the surrounding interaction points.

- The kernel is always directly along the central beam axis, i.e. there is no kernel tilting due to divergent beams.

2.2.2.3 Scatter Dose

The relative dose rate along the beam axis from scattered radiation is calculated by convolving the TERMA along the beam axis with a scatter kernel. The scatter kernel is found by least squares fitting of a double exponential to the kernels in an inverse

convolution problem. The scatter kernel is pre-calculated and stored in tables used by the algorithm.

The convoluted relative scatter dose along the beam axis is used to scale pre-calculated scatter dose profiles perpendicular to the axis and normalized to 1 at the central point. The depth scatter dose curve and the scatter dose profile are both pre-calculated using Monte Carlo methods in an 80mm water phantom.

The following approximations are considerations are made:

- One lateral profile and one kernel are used for each collimator size.

- The convolution is performed along the central axis for the beam.

- The size of the scatter dose profile is scaled with a geometric factor depending on the distance to the source.

- The kernel is not scaled due to tissue heterogeneities between the interaction points and the dose deposition points.

- The dose deposition at a point is scaled with the relative electron density to water and the inverse relative mass density to water at that point

- The relative mass and electron densities are defined in the same way as for the primary dose.

The calibration dose rate in a homogeneous water sphere is determined by a measurement of the largest collimator size (16mm for the Perfexion). A calibration factor relates the measured calibration dose to the calculate dose. In addition to the calibration factor, an output factor relates the dose for the largest collimators to the other collimators.

Equation 2.2 Convolution Algorithm

$D_i(\bar{r}) = \dot{D}_{center}\left(\omega^{c,r} / (\Sigma n^r \omega^{=16,,r})\right)(d_{i,pri}(\bar{r}) + d_{i,sca}(\bar{r}))t$, where

$$d_{i,pri}(\bar{r}) = (\eta(\bar{r})/\rho(\bar{r})) \iiint T^{c,r}(\bar{s})\rho(\bar{s})c^2 h_{pri}(c(\bar{r}-\bar{s}))d^3s$$

$$T^{c,r}(\bar{s}) = (\eta(\bar{s})/\rho(\bar{s}))\, g^2_{dz} \exp(\mu_0(80-d_{rad}))\, \Psi^{c,r}(d,\vartheta)$$

$$d_{i,sca}(\bar{r}) = P^c_{sca}(d)\,(\eta(\bar{r})/\rho(\bar{r})) \int T^{c,r}(s)k^c_{sca}(s-z)\eta(s)ds$$

$D_i(\bar{r})$	The dose rate at the point $\bar{r} = (X_{ip}, Y_{ip}, Z_{ip})$ from the source i
t	Irradiation time
$\bar{s}$	Coordinates of the interaction points
$d_{i,pri}(\bar{r})$	The contribution from the primary, i.e. un-scattered photons to the relative dose rate at the point $\bar{r}$ from the source i
$D_{i,sca}(\bar{r})$	The contribution from the scattered photons to the relative dose rate at the point $\bar{r}$ from the source i
$\dot{D}_{center}$	The dose rate is measured at the center of an 80mm spherical water phantom with all the sectors having the 16mm collimator. It includes the exponential attenuation in time due to the decay of the source. This factor relates the calculated dose rate with the measured dose rate
$\omega^{c,r}$	The output factor for the specific collimator size c and ring r. it is normalized to the 16mm collimator in the second ring
n^r	The number of sources in the ring r
μ_0	The linear attenuation coefficient for primary cobalt energies
$\eta(\bar{r})$	The relative electron density to water at the point $\bar{r}$
$\rho(\bar{r})$	The relative mass density to water at the point $\bar{r}$ calculated from the electron densities
d_{rad}	The radiological distance from the source position to the calculation point
c	The radiological length between the interaction point and the deposition point
g^2_{dz}	The inverse square that models the divergent photon field Where $g_{dz} = d_{sf}^{c,r} / (d_{sf}^{c,r} - dz)$ $d_{sf}^{c,r}$ is the source to focus distance for specific collimator size c and ring r dz is the distance along the beam axis from the point of focus to the intersection with the line that is perpendicular to the beam axis and connects to the point
$\Psi^{c,r}(d,\vartheta)$	Transverse fluence profile for the collimator size c and ring r
$T^{c,r}(\bar{s})$	The energy per unit mass released at the point $\bar{s}$ for the collimator size c and ring r
$T^{c,r}(s)$	The energy per unit mass released along the main axis of the beam at depth s for the collimator size c and ring r
h_{pri}	The primary kernel. The kernel is generated using Monte Carlo methods
k^c_{sca}	The scatter kernel for the collimator size c

$P^{c}_{sca}(d)$	The scatter dose rate profile. One profile is used for each collimator size c. The profiles are symmetric around the beam axis

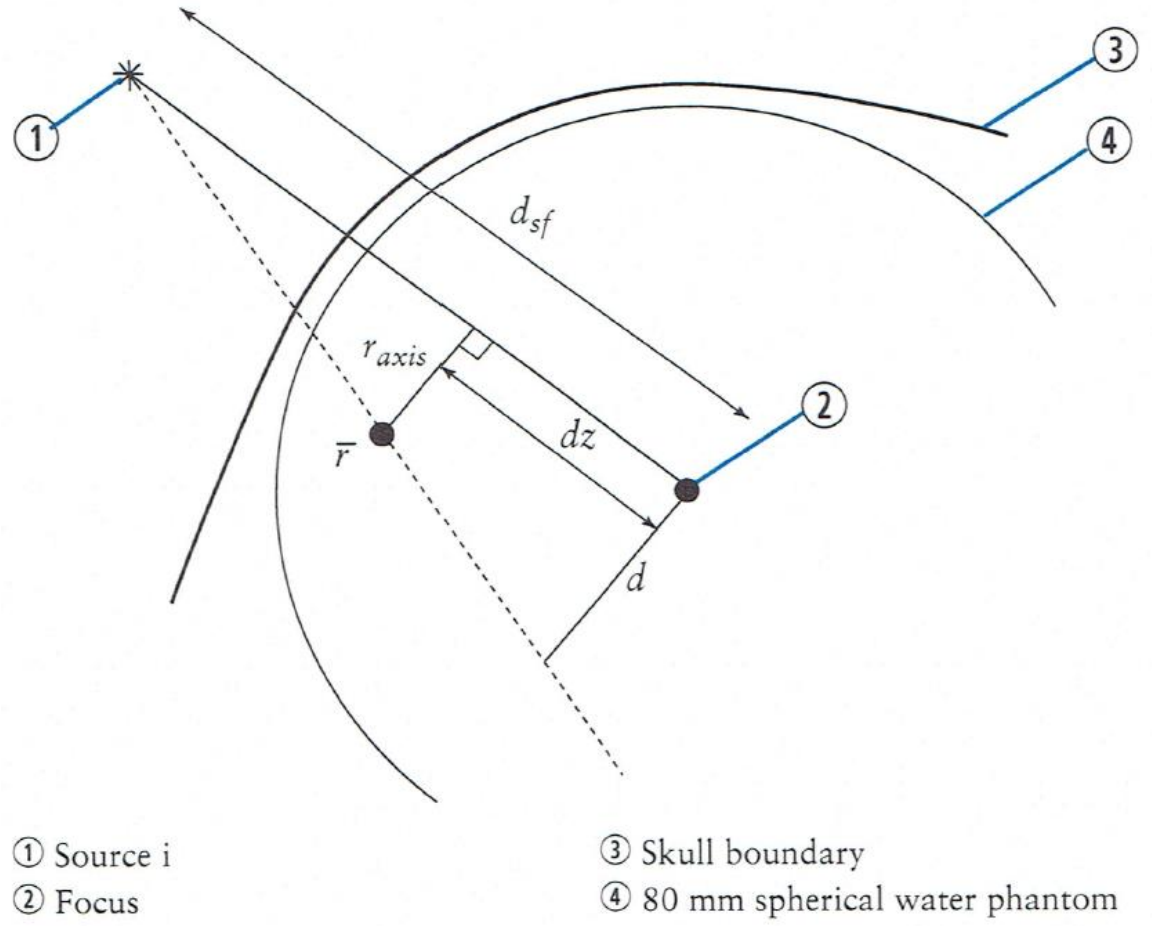

Fig 2.8 Geometry of beam in skull for Convolution algorithm

2.3 Small Field Dosimetry and Radiochromic Film

Radiation fields of the small size capable of being achieved with the Gamma Knife can require specialized dosimetry. A “small field” is generally defined as a field size of less than 3 by 3 centimeters-squared. The 3x3 guideline applies to clinical linear accelerator beams with a peak output of 6 MV, as opposed to the average energy of the Gamma Knife beams of 1.25 MeV. No specific guidelines exist for lower therapy energy

levels like these. The largest field available with the Gamma Knife, for a single shot, is 16 millimeters in diameter, which fits the definition of a small field.

In physics terms, a small field is one in which the lateral electronic equilibrium is not maintained, i.e. field flatness is compromised. In this case, the field size is smaller than the average range of the secondary electrons, resulting in charged particles leaving the dosimetric region of interest not being replaced by other charged particles entering the volume.

There are three primary parameters that make small field dosimetry difficult; the penumbra, lateral electron range, and detector size. Dose measurement under non-equilibrium conditions is challenging, one reason being the finite size of dosimeters and the fact that any dosimeter necessarily perturbs the field it measures. An ion chamber, for instance, relies on Bragg-Gray cavity theory, stating that the chamber is only non-perturbing if the range of charged particles is greater than the diameter of the chamber cavity. This requirement may not be satisfied with very narrow beams with steep gradients like those found in stereotactic radiosurgery. Small detectors, including micro ionization chambers (0.01 cubic centimeters active volume), diamond detectors, and thermoluminescent detectors (TLDs) are useful for measuring the dose at the central plateau of the beam, but cannot provide accurate data off-center due to the steep dose gradient which prevents charged particle equilibrium.

Dosimetry of irregular fields is typically scaled by utilizing measurements from known measured field data. The two components of the size of the beam penumbra at the edges of the field are geometric penumbra, which is caused by the fact that the source is not a point source, and radiological penumbra, due to scatter of secondary electrons and

photons. For small fields, the size of the radiation source becomes more important as the proportion of the field with the edge penumbra increases.

Because ion chambers do not provide sufficient spatial resolution for high gradient treatment planning needs, and because TLDs, even with small dimensions, are cumbersome and time-consuming and do not lend themselves to easy long term data storage, it was decided that the best approach would be to use radiochromic film for dosimetry. Silver halide radiographic film was not chosen because it is not ideal for evaluating ionizing photon beams because of large differences in sensitivity to photon in the 10-200 keV region. Radiographic films are also sensitive to room light and require wet chemical processing. As a result, a dosimeter is needed that has high spatial resolution and gives permanent absolute values of absorbed dose with acceptable accuracy. These features are available with radiochromic film. This film has very high spatial resolution and relatively low spectral sensitivity variation. In addition, the film is insensitive to visible light which offers a relative ease of handling and preparation. Care must still be taken to maintain the orientation of the film through irradiation and scanning. The film colors directly and does not require chemical processing; the film changes color when exposed to radiation. Images are formed through a dye or polymerization, in which energy is transferred from a photon or energetic particle to the receptive part of the dye or colorless photomonomer molecule. The films consist of a double layer radiochromic sensor dispersion coated on both sides of a polyester base. The transparent film responds to ultraviolet light and ionizing radiation by turning blue. This type of film shows consistent dose-coloration response from 3-100 Gy.

Previous tests in the literature, using radiochromic film in conjunction with a Gamma Knife, indicated agreement to within two percent. They concluded that the dose, dose profiles, and isodose curves obtained with radiochromic film can provide high spatial resolution of information of value for acceptance testing and quality control of dose measurements and/or calculations.

The open source software Image J (http://rsb.info.nih.gov/ij/) was used for film analysis in conjunction with a professional grade Epson flatbed scanner.

Chapter 3
Planning and Dosimetric Comparison of the Gamma Knife Convolution and TMR 10 Algorithms

3.1 Abstract

Purpose/Objectives: To compare the dose distributions for identical treatment plans calculated by the Gamma Knife TMR 10 and convolution algorithms and measured with film dosimetry.

Methods/Materials: An anthropomorphic head phantom was CT imaged with EBT2 film placed between each of seven axial sections. The resulting data set was used to plan three 16mm collimated targets on the Gamma Knife Perfexion, with each target centered on a film plane. Target 1 was placed within a homogeneous region while Targets 2 and 3 were placed in heterogeneous regions, i.e. tissue-air and bone-tissue interfaces, respectively. Plans using the same targets were made using both the TMR 10 and convolution algorithms. The prescription was delivered to the phantom using the TMR 10 treatment plans after which the convolution treatment plans were adjusted to result in identical treatment times, thus ensuring identical dose delivery. Film dosimetry was done to determine actual dose delivered at target center and was compared to the predicted dose for each algorithm.

Results: While there was strong correlation between both algorithms, the convolution algorithm predicted a higher delivered maximum dose than TMR 10, up to 2.5% higher in homogeneous tissue and up to 7% near an air cavity. Film dosimetry results were

consistent with the convolution algorithm predictions, with an error of less than three percent.

Conclusions: The Gamma Knife convolution algorithm predicts delivered dose to a clinically acceptable level, which was confirmed by film dosimetry. However, film in an anthropomorphic head phantom may not be adequate to measure the most significant differences between the two algorithms. Precise stereotactic treatments will require precise dosimetry, and a phantom developed specifically with Gamma Knife geometry in mind may be necessary to fully characterize the dosimetry at anatomy interfaces.

3.2 Introduction

The TMR 10 dose calculation algorithm is the currently accepted clinical standard for the Gamma Knife Perfection. Treatment planning using this algorithm uses the assumption that the entire contoured volume is of unit density and water equivalent, neglecting any heterogeneities present that may change the characteristics of the incident radiation beam. For the TMR 10 algorithm, the contoured volume, namely the patient head in clinical practice, is approximated using a semispherical three-dimensional water phantom based on 24 predefined measurement points on the patient skull. Dose calculation from a single radiation source is calculated using the strength and coordinates of the Cobolt-60 source relative to the calculation point, contoured volume measurements, and Monte Carlo based beam profiles for the respective beam collimator size. The total dose at the point is then calculated to be the summation of all 192 sources. The TMR 10 algorithm is considered clinically sufficient for targets in the center of the brain, but loses accuracy at peripheral and heterogeneous locations.

A convolution-based dose calculation algorithm is included in the current Leksell Gamma Plan distribution, but is not used clinically. The algorithm was developed as a tool to address several objectives, namely a more reliable way to define the skull shape, a more accurate scattered dose calculation, and inhomogeneity dose correction within the volume. Inhomogeneity correction in dose calculations is needed because different areas of the body have different physical and radiological properties. Because treatments are becoming increasingly conformal around tumors, the potential for over and under dosing tumor volumes and critical structures is increased. Structures relevant to the Gamma Knife that are radiologically different from water include oral cavities, teeth, sinuses, nasal passages, and bone.

The experiment is intended to compare the generated plans and predicted dose distributions using the TMR 10 and Convolution algorithms, and to dosimetrically verify the generated plans using an anthropomorphic head phantom and EBT2 film.

3.3 Methods and Materials

In order to compare the dose calculations of the TMR 10 and Convolution algorithms, an anthropomorphic head phantom (randophantom) was CT imaged according to accepted clinical parameters with EBT2 film placed between each of seven axial sections. The EBT 2 film is radiologically sensitive and accurate in all ranges of dose typically seen in a Gamma Knife treatment. The resulting data set was used to plan three 16-millimeter collimated targets on the Gamma Knife Perfexion, with each target centered on a film plane at a different location.

- Target 1 was placed within a homogeneous region of the phantom
- Target 2 was placed at a tissue-air interface
- Target 3 was placed at a tissue-bone interface

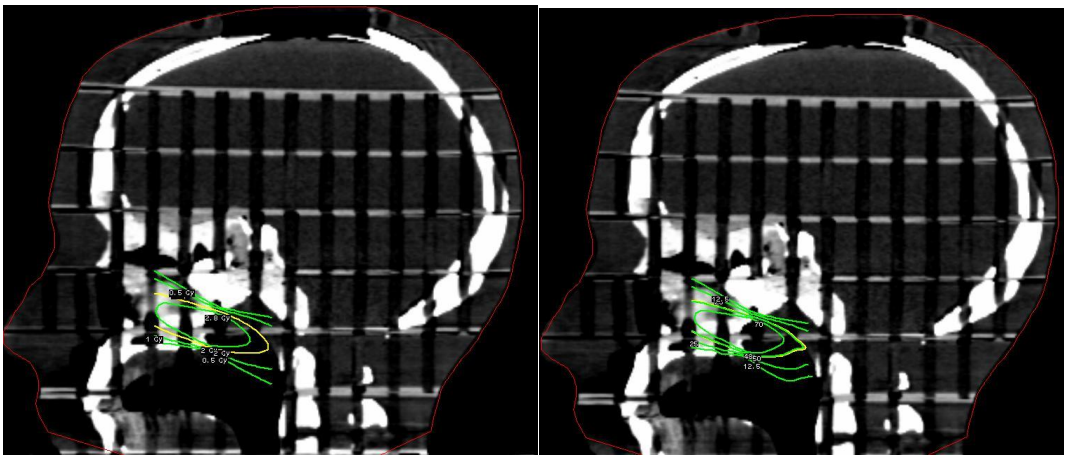

Fig 3.1. Target 2, centered at tissue-air interface, TMR 10 plan (left) and Convolution plan (right)

Plans using the same targets were made using both the TMR 10 and Convolution algorithms. Each shot, or selected beam parameters for a single location, was a single sector of twenty-four sources, which is the least number of sources that can be utilized. This beam setup was chosen in order to directionally bias the beam to maximize and effect on the dose distribution by the heterogeneous media. The TMR 10 and Convolution algorithms were compared based on predicted dose distribution in two sets of experiments for each of the three target varieties.

For the first set of experiments, all plans had identical target parameters, including sector selection and target prescription. Since the TMR 10 and Convolution algorithms use different methods, namely the Convolution algorithm taking heterogeneities into account, this could result in unequal treatment times, meaning different doses delivered to the target. The plans were delivered to the phantom and film dosimetry was done to determine how accurate the delivered dose was compared to planned dose, as well as to determine is significant heterogeneities result in clinically significant differences between TMR 10 and Convolution determined treatment parameters.

For the second set of experiments, the Convolution treatment plans were adjusted to result in identical treatment times to those of the TMR 10 plans, thus ensuring identical dose delivery. Since there is only a single shot of radiation delivered and collimator sizes were not changed during irradiation, treatment time correlates directly to dose delivered to the target. Film dosimetry was done to determine actual dose delivered at target center, and delivered dose was compared to the predicted dose for each algorithm to determine how accurate delivered dose was compared to planned dose, as well as how much at

target could be under or over dosed by using the TMR 10 homogeneous algorithm in a heterogeneous medium

Film dosimetry was done by first acquiring an H&D curve using EBT 2 film from the same lot of film used in the experiment. Pieces of film inside the Elekta Gamma Knife spherical phantom were irradiated using a 16-millimeter collimated shot for several different known periods of time. Because the dose rate at isocenter is known from machine acceptance testing, an absolute dose for each time interval can be calculated.

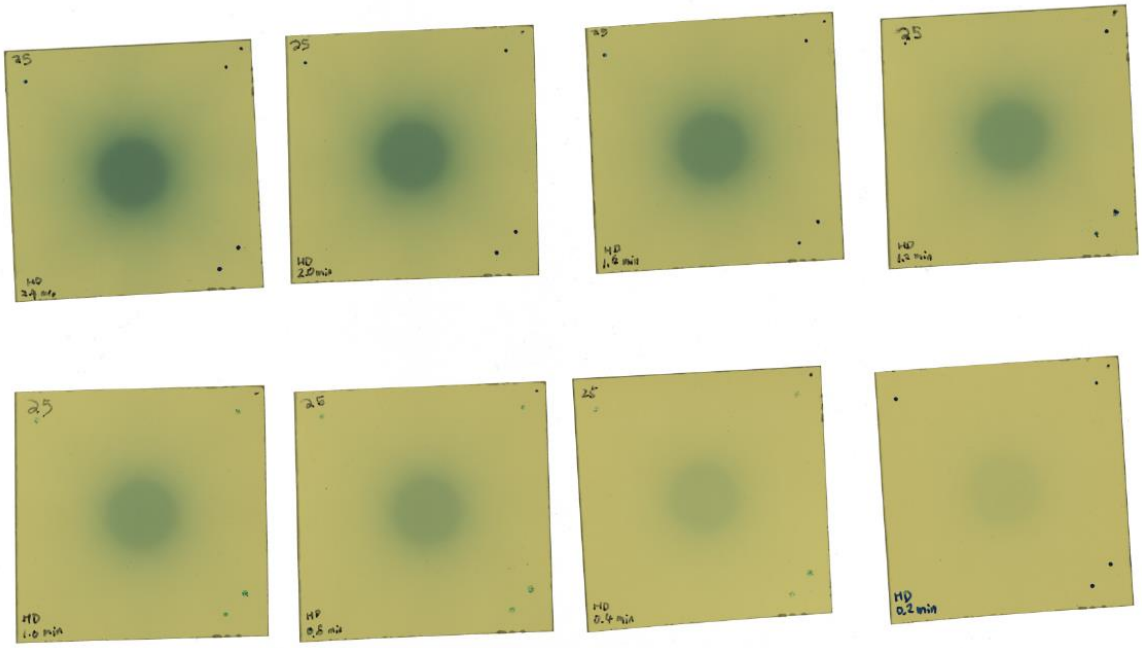

Fig 3.2. Irradiated Film for H&D Curve

Table 3.1 H&D Curve Data		
Tx Time (min)	Dose (Gy)	Pixel Value
0.2	0.647	24.9541
0.4	1.194	28.4462
0.8	2.588	35.9818
1.0	3.235	38.8832
1.2	3.882	42.3801
1.6	5.167	50.2815
2.0	6.47	57.6570
2.4	7.764	63.3568
Dose = $-0.0003x^2+0.204x-4.2937$, where x=pixel value		

The EBT 2 film was then scanned with a flatbed scanner accepted for clinical use, and the images were then imported into an image analysis software called ImageJ. The images were separated into the red, green, and blue color channels. Since EBT2 film responds in the red channel, we could use the red channel data to correlate back to dose delivered. Average intensity of the red channel in a consistently sized area in the center of each film was used as the intensity of the maximum dose. We know the dose delivered to each piece of film, therefore we can correlate the average red value intensity to a dose for each irradiated film. In this way, a dose-response curve was generated, and the 2nd degree equation of the best fit line could be used to determine dose delivered during the experiment for any given treatment time.

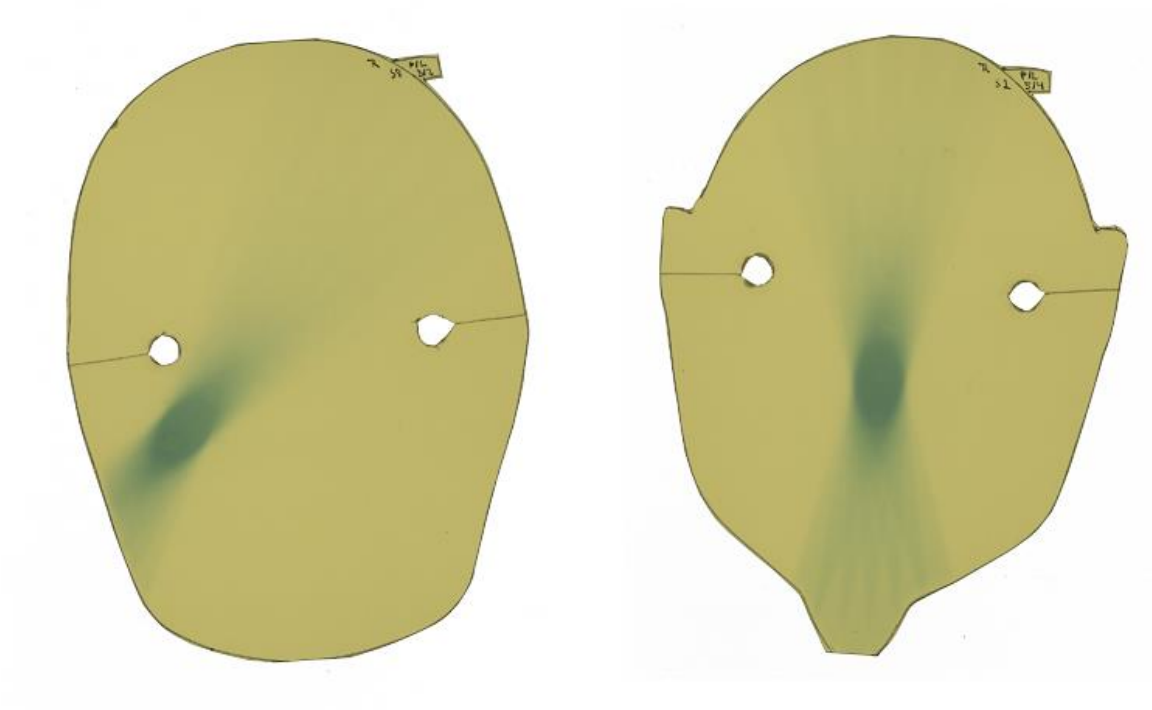

Fig 3.3. Irradiated randophantom films, showing directionality of treatment beams

3.4 Results

With three targets in different regions of the head phantom, we wanted to see what effect, if any, the extreme heterogeneities of a tissue-air and tissue-bone interface would have on the dose calculations of the two algorithms. The homogeneous target was included to see how close the algorithm predictions were when there were as little heterogeneities in the beam path as possible. While there was strong correlation between both the TMR 10 and Convolution algorithms, the Convolution algorithm predicted a higher delivered maximum dose than did the TMR 10 algorithm, up to 2.5% higher in homogeneous tissue and up to 7% near an air cavity interface. Repeated planned locations were consistent with these results. Tabulated data are included below.

Film dosimetry results to comparing predicted to delivered dose in all cases were more consistent with the Convolution algorithm predictions, with an error of less than 3 percent, which is within clinically accepted tolerances. However, the TMR 10 algorithm was also within clinically accepted tolerances, with the exception of one case of a large tissue-air inhomogeneity. In this case, more robust dosimetry than simply film on one place would be needed to determine the extent of the discrepancy.

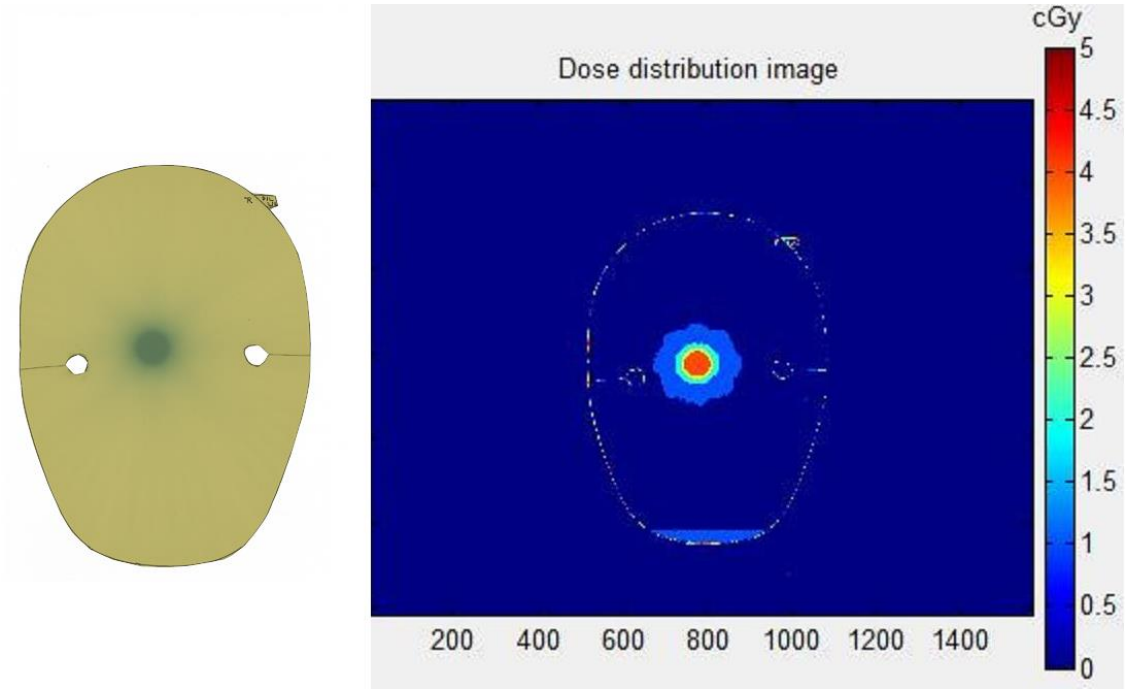

Fig. 3.4 Irradiated randophantom film and corresponding ImageJ dose map

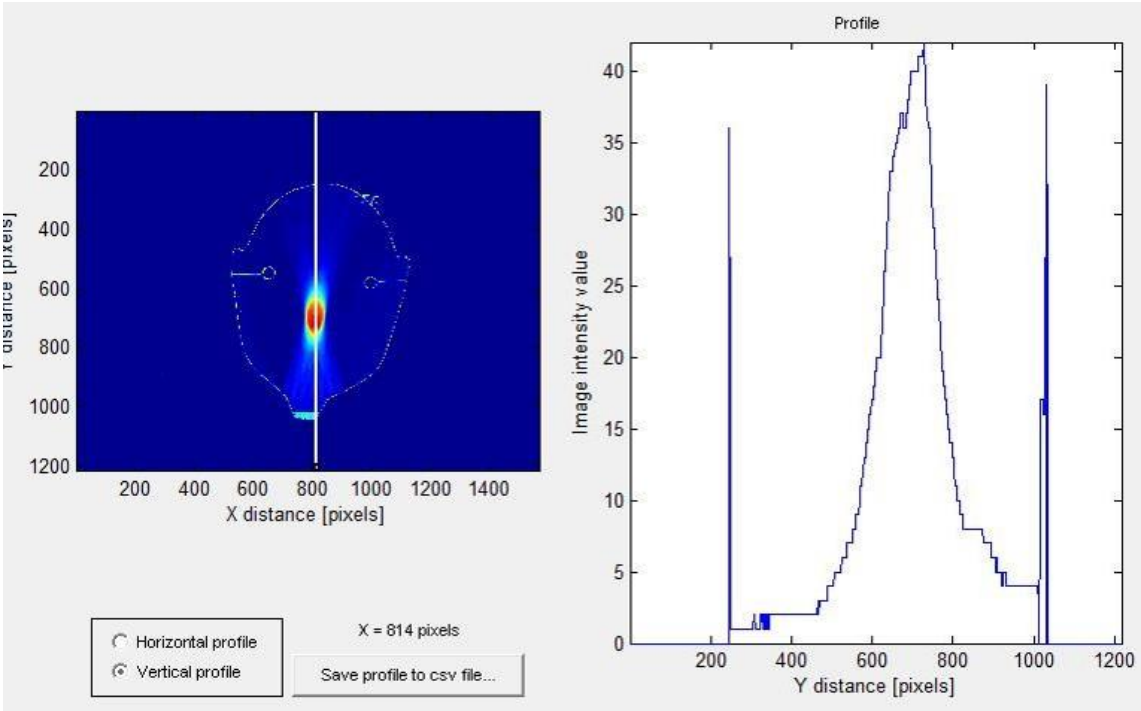

Fig 3.5. Target 2 Dose Profile and Dose Map

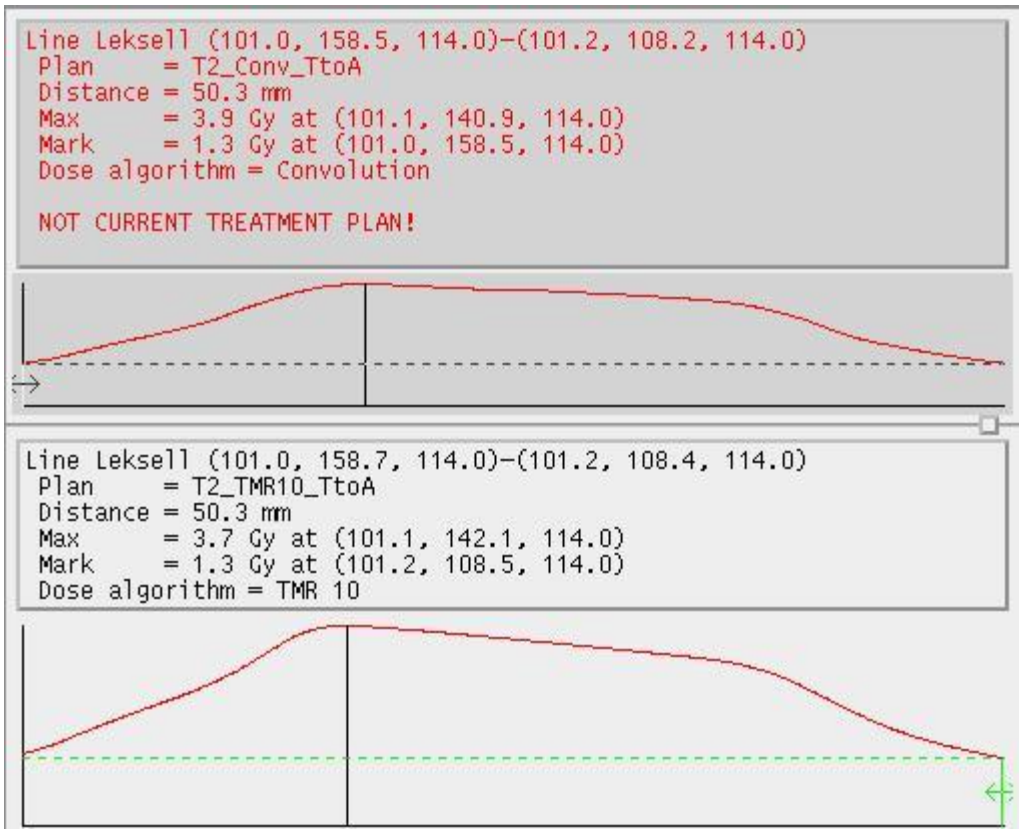

Fig. 3.6 Screen grab showing dose at a line drawn through the width of Target 2 (tissue/air) for both TMR10 (bottom) and Convolution algorithms (top)

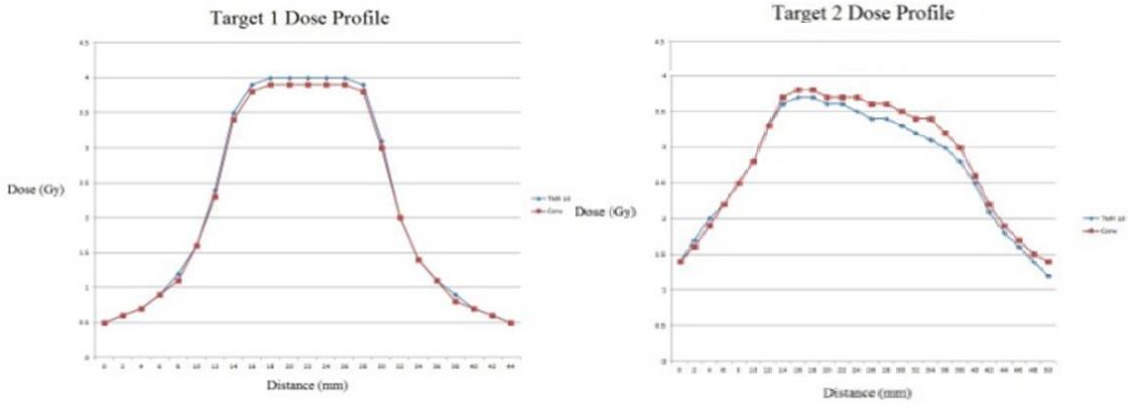

Fig 3.7 Comparison of dose profiles for TMR10 and Convolution algorithms for Target 1 (homogeneous tissue) and Target 2 (tissue-air interface)

Table 3.2 Dose Values at Multiple Points along a line through randophantom target				
	Homogeneous Target		Tissue-Air Target	
Point	TMR 10 Dose (Gy)	Convolution Dose (Gy)	TMR10 Dose (Gy)	Convolution Dose (Gy)
1	0.5	0.5	1.4	1.4
2	0.6	0.6	1.6	1.7
3	0.7	0.7	1.9	2
4	0.9	0.9	2.2	2.2
5	1.2	1.1	2.5	2.5
6	1.6	1.6	2.8	2.8
7	2.4	2.3	3.3	3.3
8	3.5	3.4	3.7	3.6
9	3.9	3.8	4.0	3.7
10	4	3.9	4.0	3.7
11	4	3.9	3.9	3.6
12	4	3.9	3.7	3.5
13	4	3.9	3.6	3.4
14	4	3.9	3.5	3.3
15	3.9	3.8	3.4	3.2
16	3.1	3	3.4	3.1
17	2	2	3.2	3
18	1.4	1.4	3	2.8
19	1.1	1.1	2.6	2.5
20	0.9	0.8	2.2	2.1
21	0.7	0.7	1.9	1.8
22	0.6	0.6	1.7	1.6
23	0.5	0.5	1.5	1.4

3.5 Discussion and Conclusion

It was expected that there would be little difference between the two planning algorithms in the homogeneous tissue. The TMR 10 algorithm is validated on a regular basis through clinical quality assurance and is very accurate in homogeneous tissue. As hypothesized, the two algorithms did show clinically significant differences at the tissue/air interface. The maximum dose delivered as well as the dose distribution were different. Absolute dose at a point could be dosimetrically confirmed, but it is difficult to

verify the dose distribution due to the large gap of seven centimeters between axial film planes.

The high resolution of film dosimetry is very appealing for measuring high gradient radiation found in Gamma Knife treatments, but because the dose falloff is significant over a very short distance, dosimetry methods including phantoms that are normally used on other linear accelerator systems are difficult to use on the Gamma Knife, and the current Gamma Knife specific dosimetry equipment is designed only to validate the TMR 10 algorithm in a homogeneous medium, and is not suitable to verify the Convolution algorithm in a heterogeneous medium.

The Gamma Knife Convolution algorithm predicts maximum delivered dose to a clinically acceptable level which was confirmed by film dosimetry. However, film in a an anthropomorphic head phantom with film placed more than one centimeter apart may not be adequate to measure the most significant differences between the TMR 10 and Convolution algorithms. Precise stereotactic treatments require precise dosimetry, and a phantom developed specifically with Gamma Knife geometry in mind may be necessary to fully characterize the dosimetry at radiologically disparate anatomy interfaces.

Chapter 4
Development of a Novel Heterogeneous Gamma Knife Phantom and Its Use Evaluating the Gamma Plan Convolution Algorithm

4.1 Abstract

Purpose: The purpose of the study was to develop and use a novel phantom to evaluate the accuracy and usefulness of a Leksell Gamma Plan convolution-based dose calculation algorithm compared with the current TMR10 algorithm.

Method: A novel phantom was designed to fit the Gamma Knife G Frame which could accommodate various materials in the form of one inch diameter, cylindrical plugs. The plugs were split axially to allow EBT2 film placement. Film measurements were made during two experiments. The first utilized plans generated on a homogeneous acrylic phantom setup using the TMR10 algorithm, with various materials inserted into the phantom during film irradiation to assess the effect on delivered dose due to unplanned heterogeneities upstream in the beam path. The second experiment utilized plans made on CT scans of different heterogeneous setups, with one plan using the TMR10 dose calculation algorithm and the second using the convolution-based algorithm. Materials used to introduce heterogeneities included air, LDPE, polystyrene, Delrin, Teflon, and aluminum.

Results: The data shows that, as would be expected, having heterogeneities in the beam path does induce dose delivery error when using the TMR10 algorithm, with the largest errors being due to the heterogeneities with electron densities most different from that of water, i.e. air, Teflon, and aluminum. Additionally, the Convolution algorithm did account for the heterogeneous material and provide a more accurate predicted dose, in

extreme cases up to a 7-12% improvement over the TMR10 algorithm. The convolution algorithm expected dose was accurate to within 3% in all cases.

Conclusion: This study demonstrated the development and manufacture of a novel stereotactic phantom and proves that the convolution algorithm is an improvement over the TMR10 algorithm when heterogeneities are present.

4.2 Introduction

A frequent responsibility of a medical physicist is to test the advertised capabilities of the devices used in or of potential use in the radiation oncology clinic. In the case of the Gamma Knife Perfexion, a Convolution algorithm that performs dose calculations that account for heterogeneities within the contoured patient volume was introduced as an additional option to the widely used and clinically accepted TMR 10 algorithm, which treats the entire contoured volume as homogeneous and water equivalent. In order to test the accuracy of the algorithm, a novel phantom, appropriate to the geometry of the Gamma Knife and that could incorporate heterogeneous material, was developed. This approach was chosen, rather than using a commercially available phantom, both as a learning experience and as a way to control costs for the project.

There are commercially available anthropomorphic head phantoms, but many are not suitable to test the accuracy and effectiveness of the convolution algorithm. A head and neck phantom developed by Webster et. Al. () was anatomically accurate, with wisely chosen materials to approximate human anatomy. Ion chamber and film measurement could be performed, but this phantom was developed to test IMRT performance and therefore large field sizes. The problems associated with small field dosimetry still remain. Another study, by Moskvin, et. Al. () demonstrated the effect of heterogeneities in the beam path with a combination of phantom measurements and Monte Carlo simulations, however they did not test the accuracy of the convolution algorithm itself.

We wanted to design and manufacture an inexpensive phantom that could incorporate a wide range of heterogeneities in order to evaluate the accuracy of the convolution algorithm in varying material arrangements. We also wanted the design to be

Gamma Knife specific, taking into account that each individual sector or any combination of sectors may want to be tested. The phantom should be able to facilitate EBT2 film dosimetry as well as ion chamber to determine absolute dose. The Gamma Knife already has a robust dosimetry system in place, so using the Gamma Knife system for absolute dose measurement facilitates creating H&D film curves that are required for film dosimetry while using the phantom. Heterogeneities within the human head anatomy are generally very small, so we wanted the heterogeneities within the phantom to be of varying sizes, both to mimic those found within the head as well as to be able to test the limits of the effects of heterogeneities within the beam, including small sizes (a few mm) to very large (0.5 inches or larger).

4.3 Methods and Materials

Due to the sector arrangement of the Gamma Knife, namely eight sectors of equal division around 360 degrees, we began our prototype as a cylindrical acrylic phantom. In order to introduce heterogeneities of various materials into the beam path of a delivered beam, we needed a phantom with exchangeable materials that could be introduced into the phantom. We achieved this by being able to interchange individual "plugs" of varying material within the phantom that were split axially to accommodate EBT 2 film. We also wanted to be able to have several heterogeneous interfaces in the same radiation shot that could approximate electron density differences similar to bone, tissue, and air interfaces.

With these parameters, we fabricated a cylindrical phantom made of acrylic, divided into three axial sections of equal thickness and diameter. The two distal sections from the G-Frame mount each had two holes, aligned section to section, and separated by

a short distance. Interchangeable plugs of varying material were machined. The materials included acrylic (for homogeneity tests), low-density polyethylene, polystyrene, delrin, Teflon, and aluminum. These materials were chosen to utilize a spectrum of physical and electron densities in the beam path, and also because they were materials routinely used throughout the literature. The plugs were split axially in order to allow EBT 2 film to be placed within the plug, and to allow combinations of half plugs of different material to increase the number and type of heterogeneities. The proximal and middle sections also had an adjoining hole to allow ion chamber measurement, along with plugs of various materials machined to accept the ion chamber to the center of the phantom. Additional plugs of any smaller size could be created by having a chosen plug size and material machined, with an outer hollow cylinder made of acrylic that could sheathe the given plug.

This combination of phantom body with interchangeable plugs accomplishes several goals. The geometry of the phantom is very simple, which means manufacturing technical expertise should not be a limiting factor. In addition, once the measurements are made and the process determined, it should be a fairly straightforward process to machine any number of plugs in many different materials. Finally, different sized plugs should also not create any hurdles, as the only parameter that would change would be the diameter of the plug. The outer "sheathe plug" should be a reasonable task for a skilled machine shop. 3-D printing of plugs is also a possibility, but the material choices are more limited.

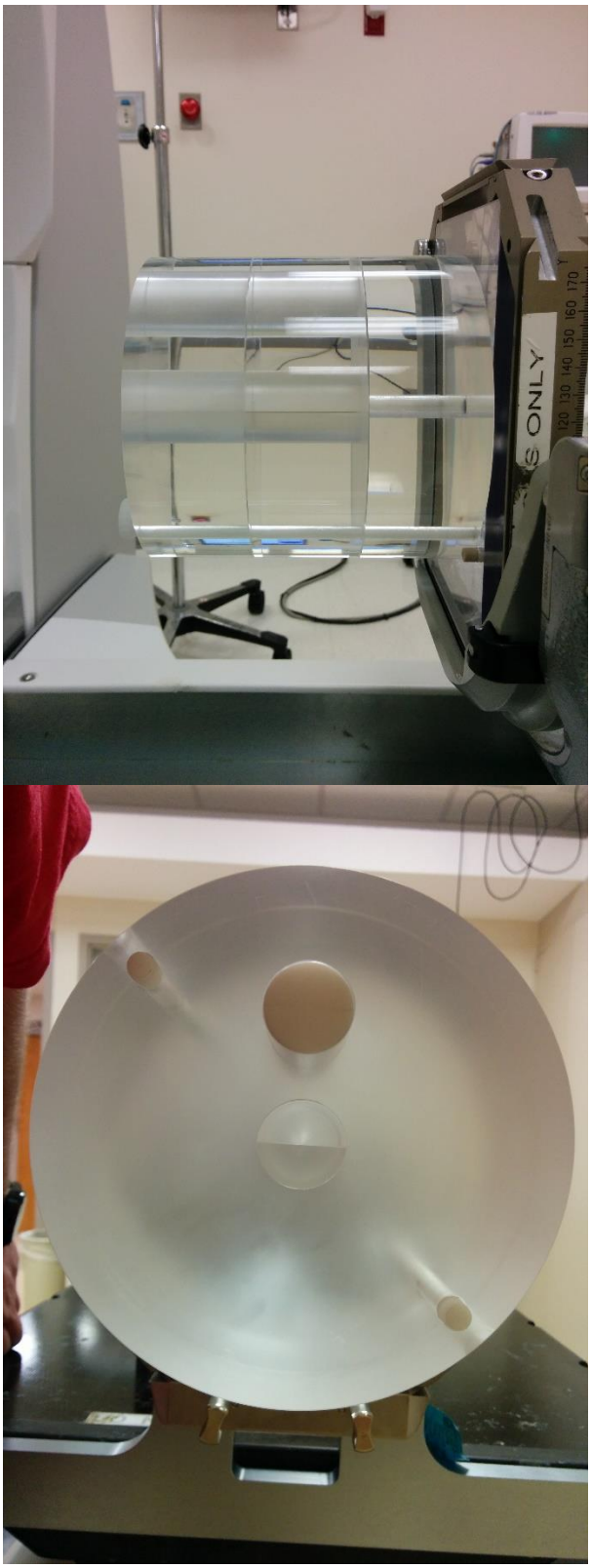

Fig 4.1. Sagital and Axial View of Phantom Attached to Gamma Knife G Frame

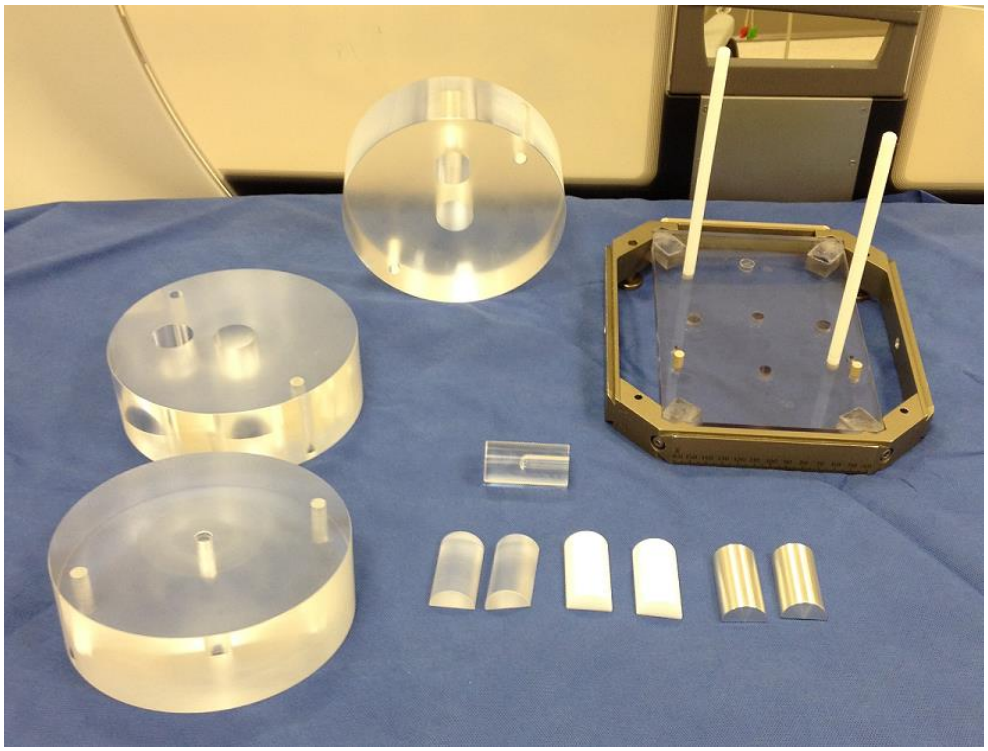

Fig 4.2. Phantom body disassembled, three plugs of different material, phantom compatible Gamma Knife couch frame

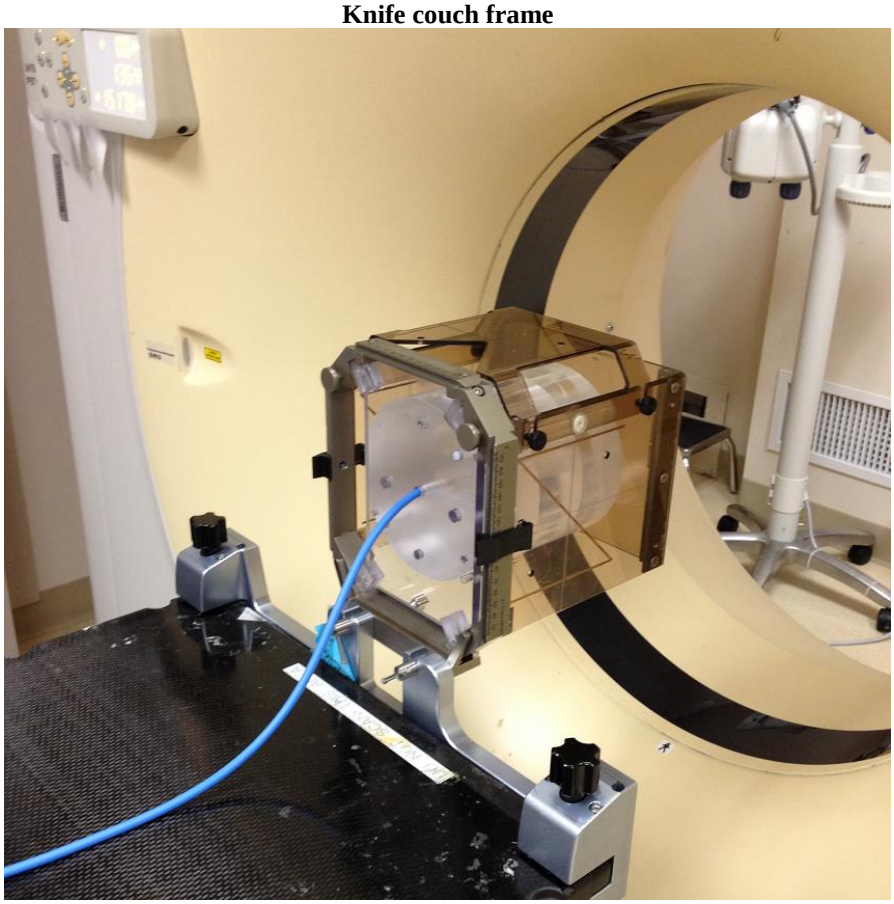

Fig. 4.3. Phantom in CT Simulator with localizer box and ion chamber

Table 4.1 Attenuation Data for Anatomy and Materials			
Sample	Density (g/cc)	μ/ρ	μen/ρ
Adipose	0.95	0.0445	0.0244
Briain	1.04	0.0443	0.0243
Soft Tissue	1 to 1.06	0.0441	0.0242
Skeletal Muscle	1.05	0.0441	0.0242
Bone	1.92	0.0418	0.0228
LDPE	0.91	0.0455	0.025
Acrylic	1.19	0.0432	0.0237
Polystyrene	1.05	0.043	0.0236
Aluminum	2.7	0.0393	0.0215
Teflon	2.21	0.0387	0.0212
Attenuation values at 2.5 MeV in cm^2/g			

Multiple arrangements of the phantom with each varying material adjacent to the acrylic body in the beam path were CT scanned on the clinic CT Simulator, and those data sets were used to plan single shot plans to the center of the phantom. The shot was a single sector with the heterogeneous plug directly upstream in the beam path from the center plug and film. Both the TMR 10 planning algorithm and Convolution algorithm were used. This initial setup and scanning is time intensive, since each combination of heterogeneities needed to be scanned and a new plan created, but once the plans were created you can run many different experiments on the same data set.

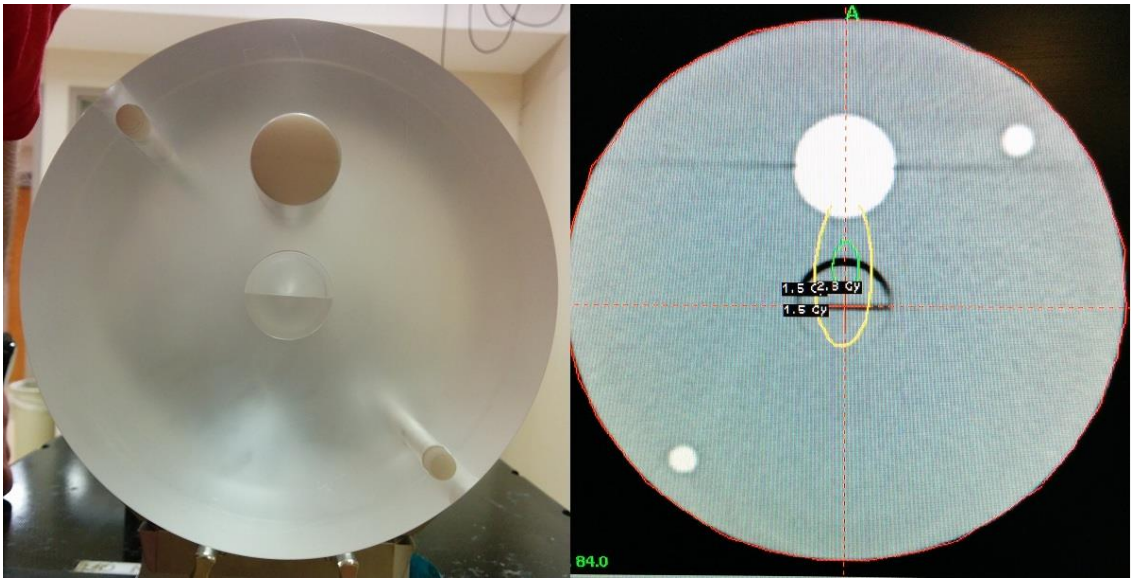

Fig 4.4. Axial view of phantom with heterogeneous plug and GammaPlan screenshot of phantom with 50% and 95% isodose lines

A first set of experiments was set up to determine the effect of heterogeneities upstream from the target on the predicted dose of the TMR10 algorithm, which treats the entire phantom volume as heterogeneous. One plan was created with a single sector shot to the film plane in the central acrylic plug, with the interchangeable heterogeneous plug upstream, and that same plan was delivered to different heterogeneous plug arrangements. The TMR 10 plan predicted dose was then compared to the measured film dose.

A second set of experiments was then set up to determine the capability of the Convolution algorithm to account for heterogeneities in the contoured volume. A plan for each heterogeneous plug arrangement was created with a single sector shot to the film plane in the central acrylic plug, with the interchangeable heterogeneous plug upstream, and each plan was delivered to the corresponding phantom setup. The Convolution plan predicted dose was then compared to the measured film dose.

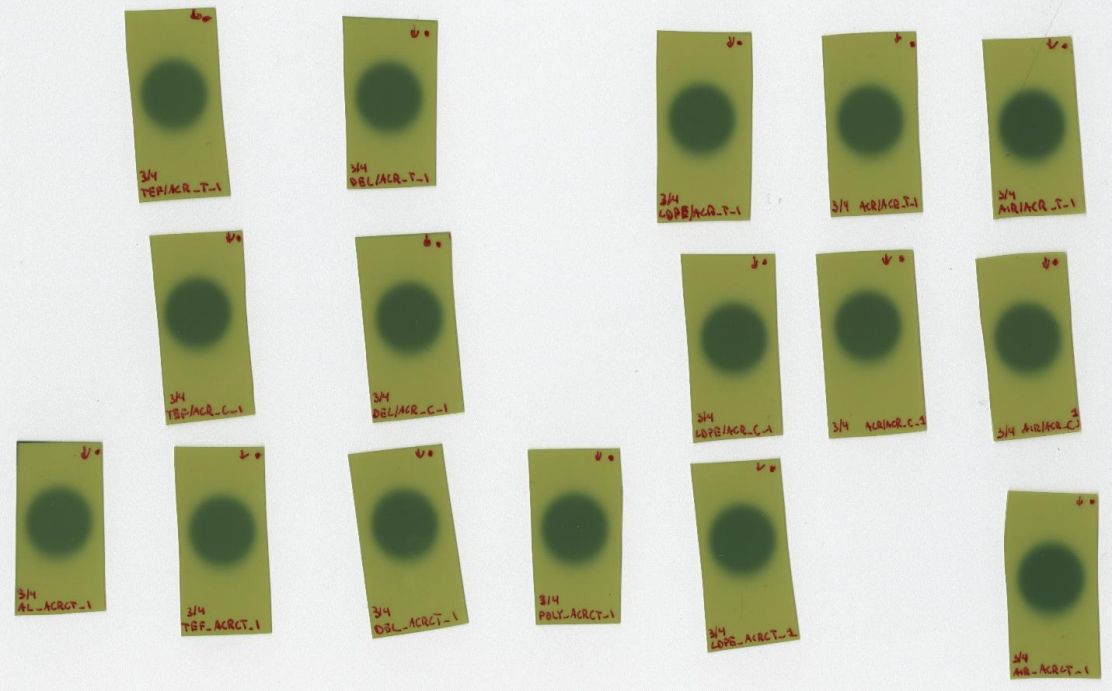

Fig 4.5 Irradiated film from central plug at central target axis with the beam passing through various heterogeneities

Film dosimetry was done by first acquiring an H&D curve using EBT 2 film from the same lot of film used in the experiment. Pieces of film inside the Elekta Gamma Knife spherical phantom were irradiated using a 16-millimeter collimated shot for several different known periods of time. Because the dose rate at isocenter is known from machine acceptance testing, an absolute dose for each time interval can be calculated. The EBT 2 film was then scanned with a flatbed scanner accepted for clinical use. The images were then imported into an image analysis software called ImageJ. The images were separated into the red, green, and blue color channels. Since EBT2 film responds in the red channel, we could use the red channel data to correlate back to dose delivered. Average intensity of the red channel in a consistently sized area in the center of each film was used as the intensity of the maximum dose. We know the dose delivered to each piece of film, therefore we can correlate the average red value intensity to a dose for each

irradiated film. In this way, a dose-response curve was generated, and the 2nd degree equation of the best fit line could be used to determine dose delivered during the experiment for any given treatment time.

4.4 Results

Table 4.2: Effect of heterogeneities upstream in the beam path on delivered dose -TMR10 predicted dose on homogeneous phantom plan, heterogeneity in delivery

Heterogeneity (upstream)	Predicted Dose (Gy)	Measured Dose (Gy)	Meas/Pred
Air	2.587	3.139	1.214
LDPE	2.587	2.779	1.074
Polystyrene	2.587	2.563	0.990
None (Acrylic)	2.587	2.582	0.998
Delrin	2.587	2.631	1.017
Teflon	2.587	2.365	0.914
Aluminum	2.587	2.280	0.880

As expected, heterogeneities in the beam path introduced dose calculation errors, with the most significant differences being up to 20% difference. It is incredibly unlikely there would be any clinical cases of heterogeneities this severe, but these results serve as an illustrative baseline to determine the effectiveness of the Convolution algorithm.

Table 4.3: Comparing TMR10 and Convolution Predicted Dose on Heterogeneous Phantom -Heterogeneity in plan and delivery

Heterogeneity and Algorithm	Predicted Dose (Gy)	Measured Dose (Gy)	Meas/Pred
Air_Conv	2.566	2.600	1.013
Air_TMR10	2.565	3.030	1.181
LDPE_Conv	2.621	2.617	0.998
LDPE_TMR10	2.565	2.656	1.035
none_Conv	2.601	2.635	1.013
none_TMR10	2.565	2.582	0.998

Delrin_Conv	2.631	2.591	0.985
Delrin_TMR10	2.565	2.489	0.970
Teflon_Conv	2.579	2.541	0.985
Teflon_TMR10	2.565	2.359	0.920

These data consistently show that the Convolution algorithm to be superior to the TMR 10 algorithm when heterogeneities are present upstream to the target. The TMR10 algorithm calculations fell outside of clinically acceptable three percent error tolerance in every heterogeneous case, and the Convolution algorithm was consistently within clinical guidelines.

4.5 Discussion and Conclusion

A convolution algorithm in the GammaPlan software was included to be used at the clinician's discretion, but the manufacturing company did not offer any advice or recommendations to its use. To evaluate its merit, a novel heterogeneous phantom was designed, fabricated, and tested. It was decided to design and manufacture the phantom in house for the learning opportunity, customization possibilities, and to keep costs to a minimum. Our phantom design is simple enough to be manufactured by many universities and hospitals with modest funds and/or manufacturing capabilities. With that said, the design is appropriate and useful for the unique geometry and irradiation mechanics of the Gamma Knife Perfexion. It allows film dosimetry and ion chamber dosimetry. A large number of material and heterogeneity size combinations are achievable with the phantom body and plug design.

This project was undertaken in order to begin to determine both if the convolution algorithm was accurate and if there were any potential clinically relevant cases where the convolution algorithm may be necessary. It was shown that the convolution algorithm dose prediction was accurate to a clinically acceptable tolerance and that there are potential extreme heterogeneities that may require its use. These cases may be very few and far in-between, but as treatments become more and more conformal, having the option to account for heterogeneities in the treatment beam may become necessary. Further testing with phantom plugs of more materials and of smaller sizes, possibly even shaped to resemble human anatomy, are logical next steps

Chapter 5
Development and Use of a System for Mouse and Rat Brain Irradiation on the Gamma Knife Perfexion

5.1 Abstract

Purpose: The purpose of the study was to implement a method for accurate mouse and rat brain irradiation using the Gamma Knife Perfexion unit. The system needed to be repeatable, efficient, and dosimetrically and spatially accurate. The Gamma Knife is well suited to this because of its capabilities delivering high dose to small targets (down to 4mm), and utilizing the G Frame allows for a high level of control over positioning.

Method: An animal platform ("mouse holder", "rat holder") was made such that it is attachable to the Leksell Gamma Knife G Frame (Fig. 1). The holder utilizes two ear bars contacting bony anatomy and a front tooth bar to secure the animal's head, with the animal's body lying in an acrylic half-tube (Fig. 2). The holder fits inside of the Leksell localizer box, which utilizes fiducial markers to register with the GammaPlan planning system. This method allows for accurate and easily repeatable setup.

For film dosimetry, a cylindrical acrylic phantom was made such that EBT2 radiochromic film can be placed axially within the phantom. We then acquired CT image sets of the holder and localizer box with both animals and the phantom. The film's response to Co60 irradiation was determined using an HD curve obtained by irradiating the same film lot in the Elekta spherical dosimetry phantom. Orientation of the film was preserved for both sample and HD films to minimize film asymmetry effects.

In this system's present capacity we are not irradiating specific tumor volumes, rather we are irradiating enough tissue to illicit a desired biological response. This means that contouring to a specific tumor is not necessary; however, we are still concerned with avoiding some anatomy like the eyes, spinal cord, and air pockets (Fig. 3).

Results: Multiple trials of the setup procedure as well as film analysis from the phantom showed that our setup is spatially accurate and repeatable. This positioning method enables a setup that is spatially accurate within <2mm superior/inferior and posterior/anterior, with virtually no rotational inaccuracy. It is also dosimetrically accurate, with a difference between predicted and measured dose of 3%. Film analysis with prescription dose and subsequently treatment time identical between rat and phantom plans showed a difference of 5%, demonstrating that our phantom is a good representation of the animal for dosimetry purposes, allowing for +/- 3mm diameter variation (Fig. 4).

Conclusion: Our method for irradiation of mouse and rat brain has been shown to be repeatable, efficient, and accurate, both dosimetrically and spatially. We can treat a large number of animals efficiently while delivering prescription doses within 3% to 5% at millimeter level accuracy. If age and size of the animals are controlled, irradiating a substantial number to gather large amounts of data requires minimal additional work beyond initial planning. Future work includes making our dosimetry model more accurate, possibly by making a more anatomically realistic phantom.

5.2 Introduction

Radiotherapy, along with surgery and/or chemotherapy, is an effective treatment protocol for patients with cancer of the brain. However, the onset and progression of radiation necrosis significantly limits the potential efficacy of the treatment. The identification of radioprotecting agents that could minimize the effects of radiation on normal tissue while not reducing the effectiveness of the radiation to tumor, would significantly improve the effectiveness of the complete treatment protocol. Unfortunately, current clinical therapeutic options for treating radiation necrosis are limited because surgical resection is often not possible due to the location of the necrosis in the brain. Radiation necrosis is a severe, late occurring (three months to ten years after radiotherapy) injury to normal tissue within and surrounding a radiation treatment site. The necrosis can lead to significant complications for patients with brain tumors. Radiation necrosis is difficult to distinguish from recurrent tumor.

A group of researchers at Washington University in St. Louis wanted to create a clinically relevant murine model of radiation necrosis, using singe hemispheric irradiation to generate late time-to-onset tissue injury, whose histology matches that of patients with confirmed radiation necrosis. This model would provide a platform for studies aimed at developing methods to identify/detect, monitor, protect against, and mitigate radiation necrosis, and distinguish it from tumor regrowth. They also wanted to investigate the effectiveness of anti-VEGF antibodies in reducing delayed-time-to-onset necrosis. In this way, the animal model could also serve as a platform for studies attempting to optimize the dosing and timing of anti-VEGF therapy.

This project was intended to provide researchers with a method for accurate, repeatable, and efficient irradiation of mouse and rat brains. Small-animal models provide a useful platform for studying many disease processes, in particular for this project the development of radiation-induced necrosis and the effects of radioprotectors and radiosensitizers. We wanted to provide the capabilities of an efficient and accurate system for small animal irradiation to a team of researchers developing a small-animal model of radiation necrosis. A well-developed model was lacking in the literature, and the Gamma Knife Perfexion unit is well suited for this because of its capabilities delivering high dose to small targets. The researchers wanted to be able to target a single hemisphere of the brain in both mice and rats which, in the case of mice, can be approximately one centimeter in width. Utilizing the G Frame system allows for a high level of control over positioning and the small aperture sizes available (down to 4mm) allow for irradiation of small target areas. In addition, both high resolution CT and MRI images are able to be utilized in the treatment planning process. The researchers had previously used the microRT system, but it did not allow for a high enough throughput of mice.

There are commercially available small animal irradiators that require a significant monetary investment that may not be feasible for many departments. In addition, current radiotherapy capabilities for humans have become increasingly sophisticated, which makes it that much harder for a relatively inexpensive and less complex small-animal irradiator to provide the same quality of radiation delivery. There are also examples in the literature of groups who have developed and constructed their own small-animal irradiators, but this is largely impractical and unnecessary for many

researchers. It requires a large investment of physics and engineering manpower, including the expertise to create a specialized cone beam CT setup appropriate for small animal imaging, as well as a dedicated treatment planning system. Utilizing a machine already in the department that is capable of delivering accurate and sufficient dose with minimal capital and time investment provides a valuable service that can be replicated by other researchers. Traditionally, animal radiation was delivered with kV photons instead of MV photons in order to avoid excessive dose buildup regions near medium interfaces, and to avoid wide beam penumbras, which can sometimes encompass the whole animal. In addition, photon energies below 100 keV could result in different dose absorption between human tissue and animal tissue, making the results of the research less relevant. It is a compelling case then to use a modern radiotherapy machine that is well equipped to deliver highly conformal dose to small targets.

Table 2
Typical properties of research devices used for small animal irradiation.

Research device	Beam quality [MeV] [a]	Dose rate [Gy/min] [b]	Irradiation technique	Collimator	Image guidance	Targeting accuracy
X-ray cabinet systems	X-rays: 0.01–0.35	1–5	fixed beam (vertical)	—	depends on device: radiography	< 1 mm–few mm
^{192}Ir MicroRT [115,116]	γ (^{192}Ir): 0.35	1–3 (300 GBq)	fixed beam (orthogonal)	collimator assembly with conical inserts	—	< 0.2 mm
SARRP Research Platform [117–121]	X-rays: 0.005–0.225	1–4	fixed beam, conformal arc	nozzle	radiography, CBCT,	0.2 mm
X-RAD 225Cx [6,122–125]	X-rays: 0.005–0.225	1–4	fixed beam, conformal arc	nozzle	radiography, CBCT	0.2 mm
MicroCT/RT system [126–128]	X-rays: 0.07–0.12	1–2	fixed beam, conformal arc	variable iris aperture	CBCT	0.1 mm
SAIGRT system [129–131]	X-rays: 0.01–0.225	1–4	fixed beam, conformal arc	flat aperture	radiography, CBCT	0.1 mm

[a] maximum energy for X-rays, mean γ and X-ray photon energy for nuclides [49].
[b] at a typical dose reference point.

Fig 5.1. Properties of commercially available small-animal irradiation devices

5.3 Methods and Materials

A custom mouse holding platform was developed in order to position and contain from one to five mice. The platform body was machined out of acrylic and was

approximately 5 millimeters thick, which is thin enough to make any radiation attenuation negligible. To be compatible with the clinical Gamma Knife imaging and positioning procedures, the holder dimensions were such that the holder could incorporate a MRI compatible frame that allows fiducial image registration with the GammaPlan treatment planning software. The platform could also be attached to the standard Gamma Knife G frame that is compatible to the stereotactic coordinate system used in clinical practice. In this way, users with standard Gamma Knife clinical plan creation training could also make plans for small animal irradiation using our platform.

To position and hold the mice, 5 acrylic, half-cylinder mouse holders were machined to fit onto the platform in consistent positions. The mice were secured using two ear bars that contact bony skull anatomy as well as a tooth bar that hooks behind the animal's teeth. Using a custom acrylic skull cap for lateral and anterior/posterior alignment, movement in all three spatial directions was minimized and positioning was reproducible from animal to animal. Mice of a consistent type, size, and weight are always used which assists accurate repositioning. The mice are anesthetized with a mixture of ketamine, acepromazine, and xylazine for periods of up to 45 minutes, which is enough time to deliver necrosis inducing radiation doses, even accounting for source strength decay over the use period.

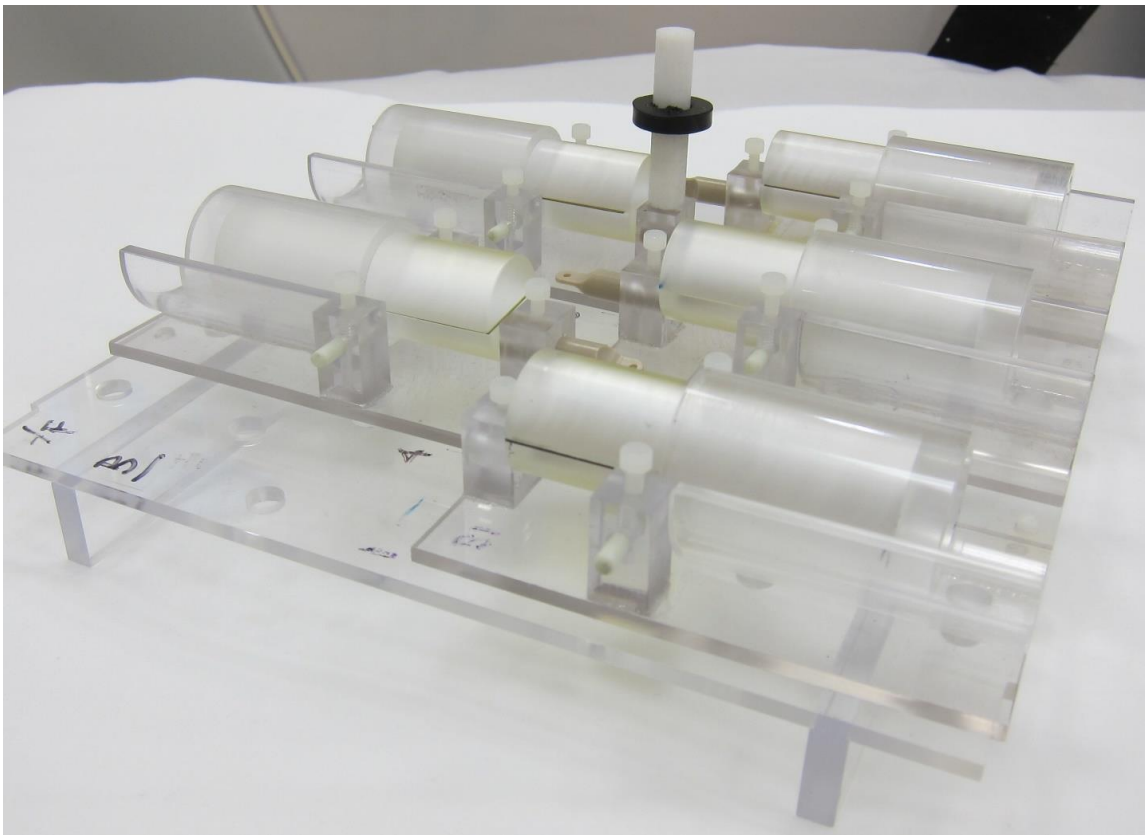

Fig 5.2. Mouse platform with cylindrical phantoms inside mouse holders

To begin the treatment planning process, 5 mice are anesthetized, positioned in individual cylindrical holders, and attached to the platform. A localizer box with fiducial markers visible on CT on both sides and the top is attached to the platform. The platform is then attached to the CT simulator couch and imaged using brain imaging parameters. The entire platform is imaged and the image data sets are transferred and imported to the GammaPlan system. Using the fiducial markers from the localizer box, the platform images can be registered to the GammaPlan stereotactic coordinate system. In this way, irradiation accuracy is limited only by animal positioning accuracy and the positioning capabilities of the Gamma Knife itself, which are quite robust.

Once a plan is created, it can be copied any number of times with any type or combination of shots required. This study utilized a four millimeter at isocenter

collimated shot, delivered to the left hemisphere of the brain. Prescription doses range from 30 Gy at 50% isodose (60 Gy maximum) to 60 Gy at 50% isodose (100 Gy maximum). This amount of radiation is more than enough to induce necrosis and maximum treatment time is approximately 45 minutes. If the shot parameters are consistent from animal to animal, new plan generation is very rapid, allowing for a large number relatively large number of mice to be treated in a reasonable amount of time.

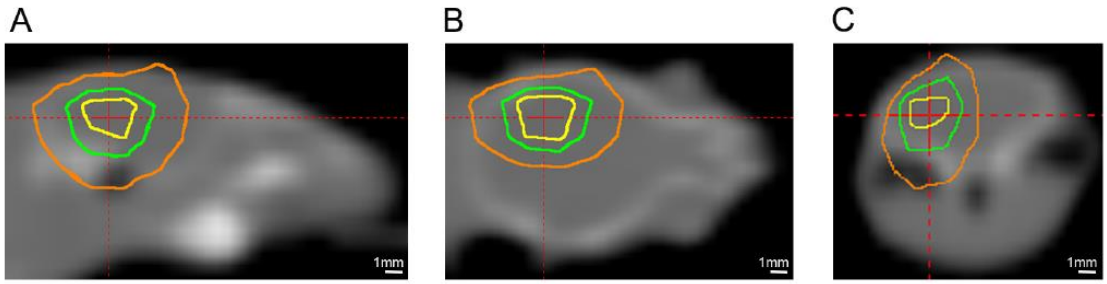

Fig 5.3. Dose contours on CT image of a mouse. Images A, B, and C show sagittal, coronal, and axial views, respectively. The isodose lines shown are 75% prescription (yellow), 50% (green), and 25% (orange). The red crosshairs show the location of the other imaging planes relative to the image viewpoint.

Dosimetry was performed utilizing cylindrical acrylic phantom of a diameter similar to that of a mouse head that fit inside the individual mouse holders. The cylinders were split axially to accommodate EBT2 film. The platform was imaged with a phantom in a holder at every position on the platform. This platform plus phantom dataset was sent to the GammaPlan and a plan was created in the same manner as a mouse plan. Shots of four, eight, and sixteen millimeters with isocenter on the film plane were planned and delivered. Film measurements and dose calculations were performed in the same manner as described earlier in this paper. Shots planned on the phantom containing platform with targets on the film plane for each position were planned and delivered. This was designed to determine if the GammaPlan algorithm was accurate while modeling the phantoms. Dose predicted was compared to dose measured at each position. Additionally, shots

planned on the mouse containing platform with targets at the previous film plane coordinates were planned and delivered. This was designed to determine how well our phantoms approximated a mouse in the calculation of the GammaPlan algorithm. Dose predicted was compared to dose measured at each position.

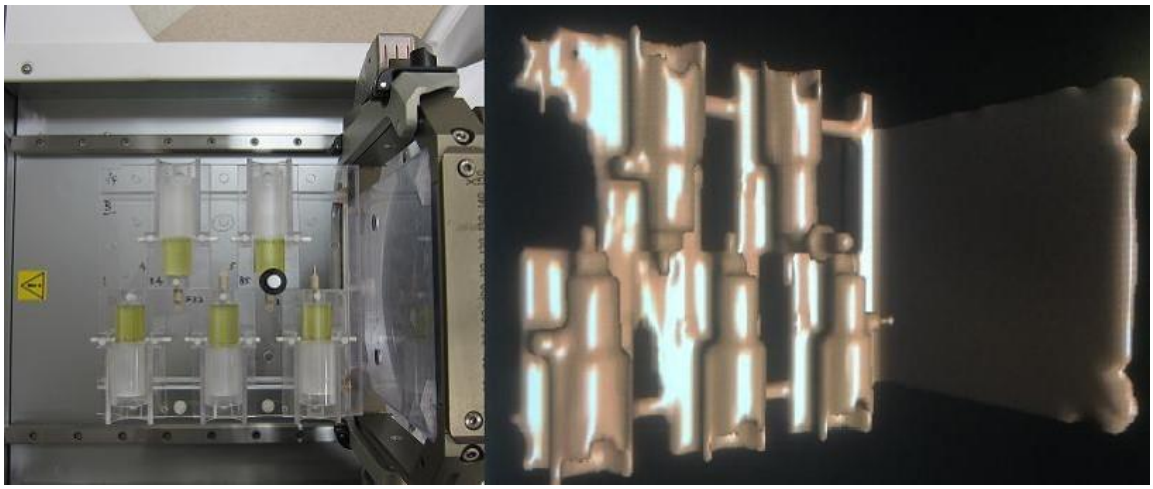

Fig 5.4. Left: Mouse holder platform with phantoms and film attached to the Gamma Knife G Frame Right: GammaPlan 3D mesh contour of phantoms

For the murine model, cohorts of mice were irradiated with single-fraction 50 or 60 Gy doses of radiation targeted to the left hemisphere. Onset and progression of radiation necrosis was monitored weekly by non-invasive in-vivo small animal MRI. MRI-derived necrotic volumes for antibody treated and untreated mice were compared.

A platform designed to accommodate a rat was also designed. This platform was entirely based off of the mouse design and had similar dimensions to accommodate the localizer box and similar animal holder features to position the rat. The rat holder was different only in that it held only one rat on the platform at one time. All experimental procedures, from imaging to localization within the coordinate system to animal

positioning, were the same as the mouse procedures. In this way, it was fairly straightforward to switch between mouse and rat experiments.

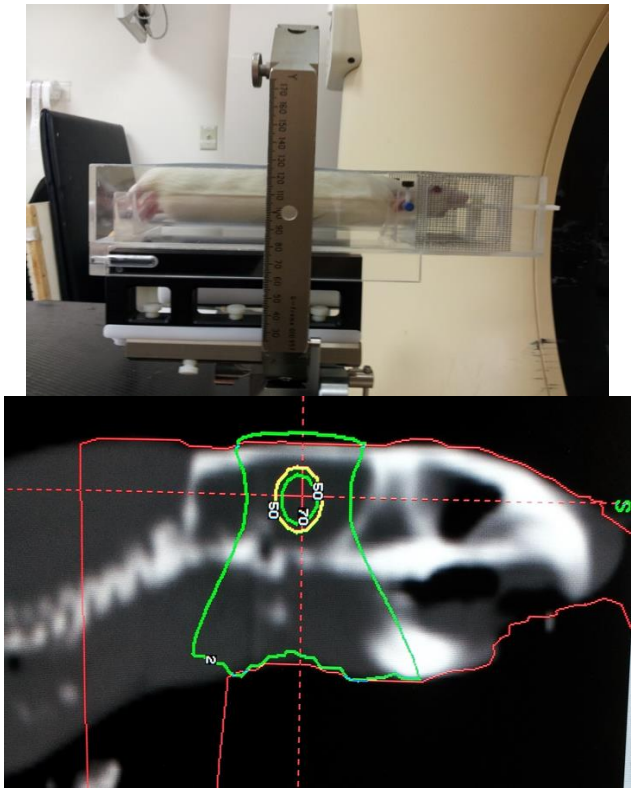

Fig 5.5. Left: Rat in holder attached to frame, Right: Prescription (yellow) and isodose of rat brain shot

In addition to brain irradiation, a small pilot study was undertaken to irradiate mouse lung. Imaging and setup was exactly the same as for all other mice, but a more contoured shot arrangement was utilized to irradiate the lungs fully but avoid nearby critical organs. The lungs were irradiated using two 4 millimeter collimated shots contoured to the left lung. The success of this project demonstrated the robust capabilities of the Gamma Knife and our animal immobilization and positioning system.

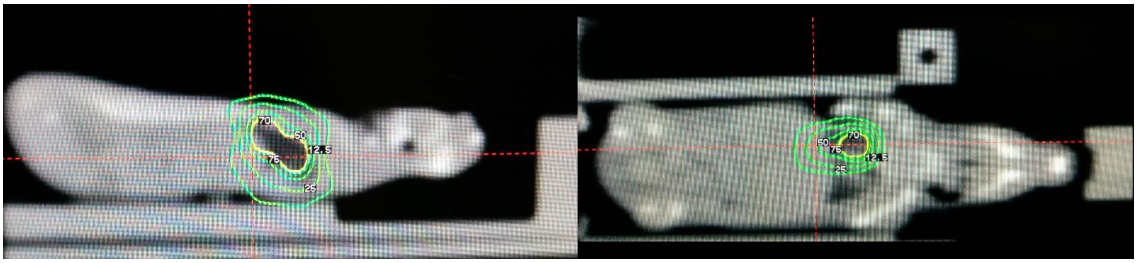

Fig 5.6: Prescription (yellow) and Isodose lines for mouse lung irradiation

All studies were performed in accordance with the guidelines of the IACUC and in accordance with protocols approved by the Washington University Division of Comparative medicine that met or exceeded American Association for the Accreditation of Laboratory Animal Care standards. Female Balb/c mice were used for the study and observed daily and weighed weekly to ensure that interventions were well tolerated.

5.4 Results

Repeated mouse positioning and measurement demonstrated that the mouse could be positioned within the holder to an accuracy in all spatial directions of less than 0.5 millimeters error. This was confirmed through physical measurement as well as visible necrosis regions when histology was performed. The positional accuracy of the Gamma Knife couch is with one-tenth of a millimeter, so positional accuracy of the mouse (and rat) and by extension shot placement is well within a tolerance that allows shot placement within a particular hemisphere of the mouse brain.

A “cross-contamination” experiment was performed to determine if a shot delivered to one position on the holder would deliver dose to a mouse at any of the other four positions. This was done by placing phantoms and film in all five holder locations and irradiating two 8 millimeter collimated shots to only one position. This was repeated

for each of the five positions. Film analysis confirmed that no non-targeted positions receives any significant dose that would affect an experiment.

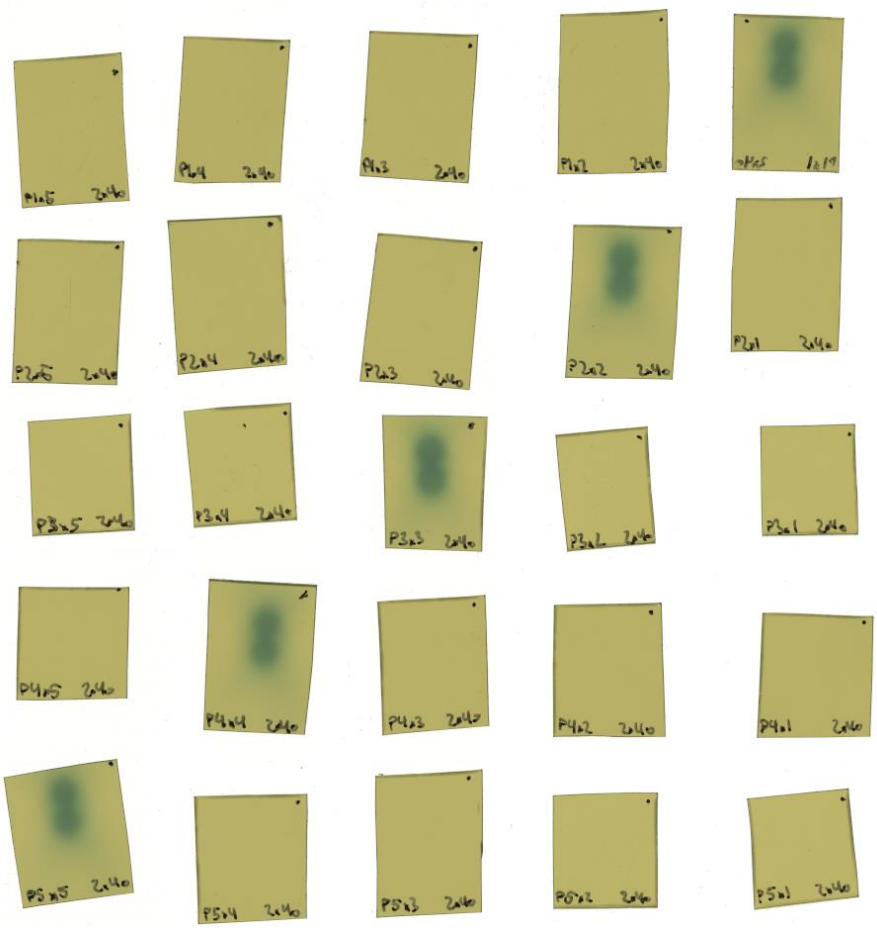

Fig 5.7: Cross-contamination experiment film

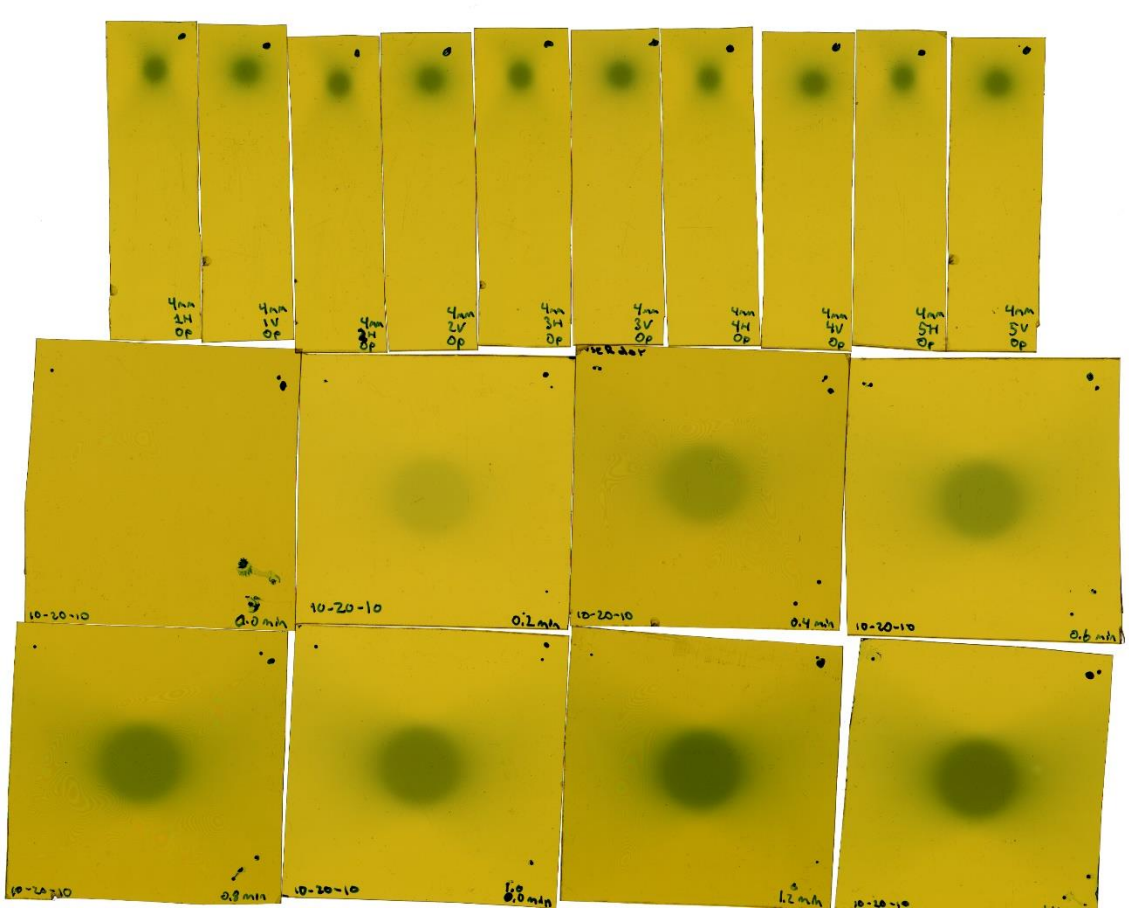

Fig 5.8: (Top row) Irradiated film from cylindrical phantom, (Bottom 2 rows) Film irradiated for H&D Curve

Table 5.1: H&D Curve Data for Mouse Dosimetry		
Dose Rate to center of Gamma Knife Phantom = 3.121 Gy/min		
Time (min)	Dose (Gy)	Pixel Value
0	0	46625
0.4	1.2484	35154
0.8	2.4968	27815
1.0	3.121	25718
1.2	3.7452	23596
1.6	4.9936	19888

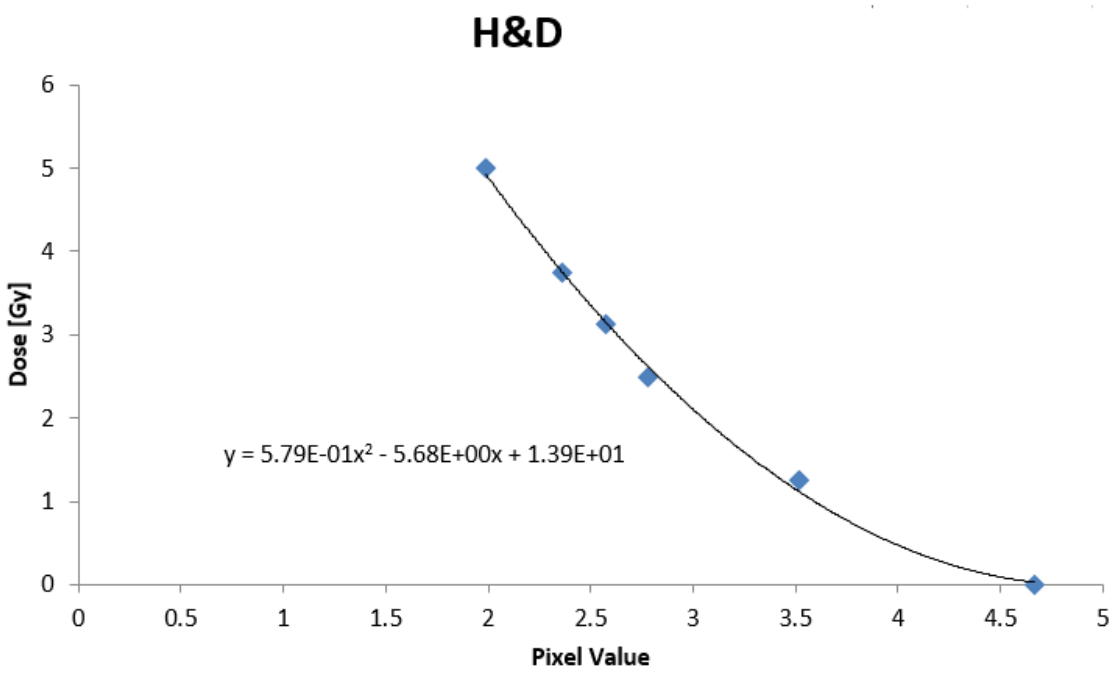

Fig 5.9: H&D Curve for mouse dosimetry experiments

Film analysis showed that when planning on a phantom plan and delivering radiation to the phantom, measured dose was within three percent of predicted dose. When planning on the mouse dataset and delivering radiation to the phantom, measured dose was within five to seven percent of predicted dose. While five to seven percent is not clinically acceptable, it was deemed to be acceptable for these experiments. Most of our experiments delivered 50 Gy to the 50% isodose line, meaning a maximum dose of 100 Gy. Five percent of prescription is plus or minus 2.5 Gy, and no experiment done compared response to doses within 2.5 Gy of one another. Any change in prescription was a change of at least 10 Gy. These measurements proved that our system was very spatially accurate and acceptably dosimetrically accurate. At the time of this writing, we have successfully irradiated over 1,000 mice and contributed to a robust murine necrosis model.

The murine model proved that our Gamma Knife procedure was effective at accurately inducing necrosis to a specified and consistent position. Additionally, because we were able to keep the dose away from critical structures, they were able to demonstrate the effectiveness of their anti-VEGF compound at delaying the onset of necrosis.

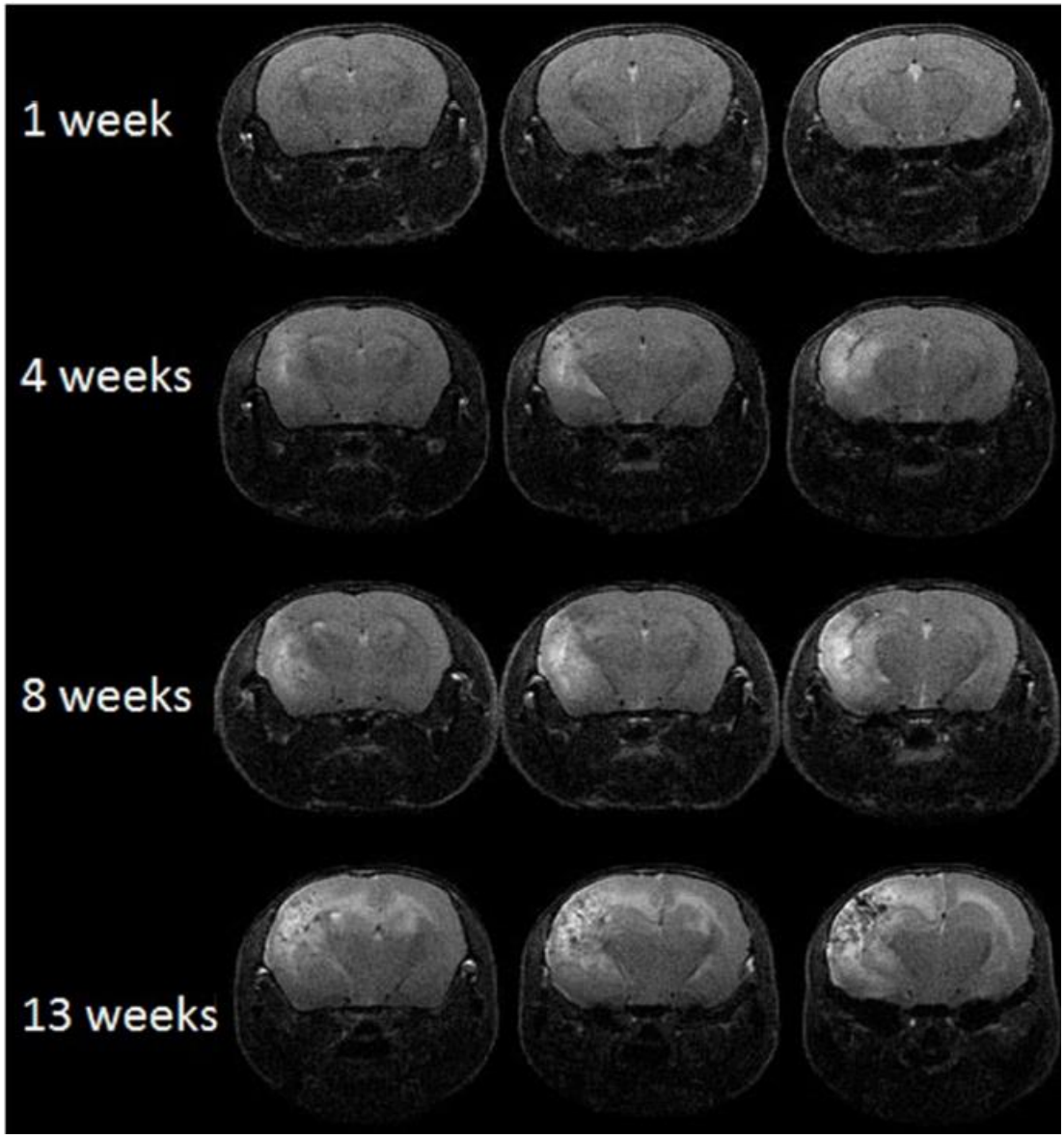

Fig 5:10 CT images of the irradiated mouse brain at various time points demonstrating induced necrosis

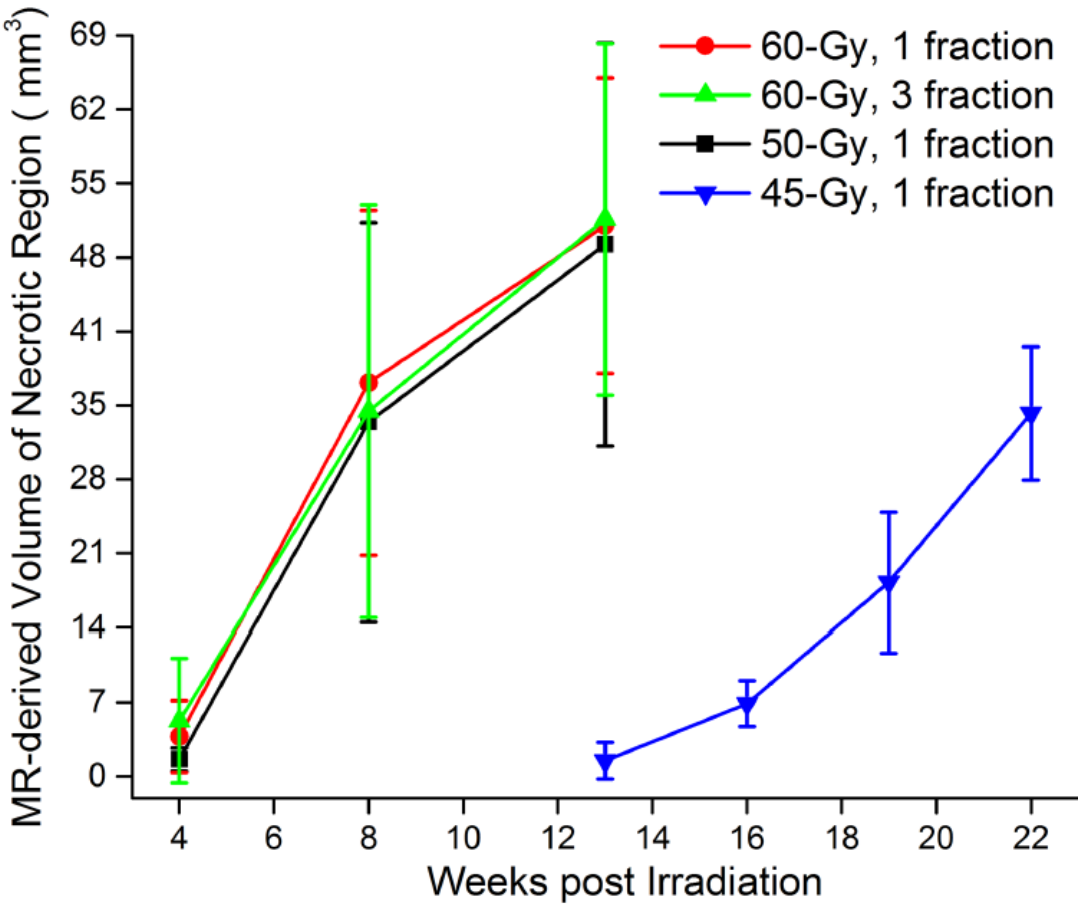

Fig 3. MRI-derived necrotic volumes. Mean volumes ± SD (n = 15), *vs*. time post-irradiation for mice irradiated hemispherically with different dose schedules: 60-Gy in 1 fraction (red), 60-Gy in 3 fractions (green), 50-Gy in 1 fraction (black) and 45-Gy in 1 fraction (blue).

Fig 5.11 Data from the research group demonstrating the effectiveness of the anti-VEGF antibodies at mitigating necrosis

5.5 Discussion and Conclusion

A research group was looking for a way to reliably and efficiently irradiate a large number of mice and rats to develop a useable and robust radiation response model. By developing a novel mouse holder and using the standard capabilities of the Gamma Knife Perfexion, we were able to offer such a service at much less of a monetary and time cost than other available options. Our system was demonstrated to be spatially and dosimetrically accurate, efficient and cost effective. While not a routine part of the radiation oncology clinic, it is part of the job of a medical physicist to offer services and

solutions related to the use of radiation in a research setting. Which this project we have done just that, to the benefit of the physicists as well as an collaborative research group.

DISCUSSION AND CONCLUSION

Throughout the course of this project we have performed duties that, while not routine, are things that are sometimes expected of a practicing clinical medical physicist. We needed to evaluate both the accuracy and usefulness of a new feature for a clinically used machine, in this case a new dose calculation algorithm for a treatment planning software. The Gamma Plan software has an included Convolution algorithm that is able to account for heterogeneities within the treatment volume, which is not a feature currently used clinically. We developed and executed a plan to compare the currently clinically accepted algorithm to the new algorithm on a planning basis, then utilized an anthropomorphic phantom coupled with film dosimetry to evaluate the planning and dose delivery accuracy of the algorithm. As a physicist, one would be expected to be able to competently evaluate any new tool or procedure and make recommendations for or against its use to the rest of the clinic.

Evaluation of a new feature to the clinical procedure may be as simple as running tried and true routine tests, or as complicated as developing a novel system for testing. In the case of our second set of experiments, we developed a novel phantom to do film and ion chamber measurements allowing us to test the accuracy of the Convolution algorithm, as well as to test the limits of when accounting for heterogeneities within the treatment volume may be necessary. We designed our phantom from the ground up to be less expensive than commercial options, reasonably easy to manufacture for a competent machine shop, and specific to the Gamma Knife Perfexion. Our phantom and plug design allowed for a large number of combinations of heterogeneous materials to be placed in

the beam path, as well as varying sizes of heterogeneities. We demonstrated the accuracy of the new Convolution algorithm, thus allowing a clinician to have confidence that a plan created using this algorithm will be delivered accurately.

We also performed another duty sometimes asked of a physicist, namely to provide expertise to assist another research team. In this case, we provided equipment design, protocol design, and dosimetry services to a multidisciplinary research team outside of the radiation oncology clinic. We developed a system to irradiate a very large number of mice to sub millimeter accuracy, successfully irradiating more than 1,000 mice over the course of three years. In addition, our system is user friendly enough that different technicians could learn the process and repeat it still retaining the same geometric and dosimetric accuracy during their experiments.

Future work would include manufacturing additional heterogeneous plugs for our phantom in order to test the limit of when accounting for heterogeneities in the beam path during a Gamma Knife treatment would be clinically necessary. Additionally, further testing of the Convolution algorithm may allow treatments to become even more conformal than they currently are, which would be clinically relevant because treatments in the brain need to be as conformal as possibly to reduce the risk of brain damage. The Gamma Knife relies on being highly conformal, and any improvement in that conformality would benefit patients by being able to treat current diseases more safely and by allowing clinicians to treat closer to more sensitive anatomy.

REFERENCES

1. AAPM, Tissue Inhomogeneity Corrections for Megavoltage Photon Beams, Report of Task Group No. 65 of the Radiation Therapy Committee of the American Association of Physicists in Medicine

2. Ahnesjö A., Collapsed cone convolution of radiant energy for photon dose calculation in heterogeneous media. Medical Physics, Vol. 16:577., 1898

3. Ahnesjö A and Aspradakis MM., Dose calculations for external photon beams in radiotherapy. Physics in medicine and biology, 44(11):R99-155, 1999

4. Ahnesjö A., A pencil beam model for photon dose calculation. Medical Physics,Vol. 19:263., 1992

5. Alvarez, P.E., A. Molineu, N. Hernandez, D. Followill, G. Ibbott Analysis of Multiple Irradiations of an Anthropomorphic Thorax Phantom Containing Lung Heterogeneities, Proceedings of 48th Annual Astro meeting

6. Charest, G., Paquette, B., Mathieu, D., Applications of Gamma Knife Radiosurgery for Experimental Investigations in Animal Models, www.intechopen.com

7. Chung, H., Chung, Y., Kim, D., Sun, P., Kuen-Tae, C., Development of a Stereotactic Device for Gamma Knife Irradiation of Small Animals, J Korean Neurosurg Soc 43, 26-30, 2008

8. Elekta. The convolution algorithm in Leksell GammaPlan 10 [white paper]. Article No 018881-01. Norcross, GA: Elekta; 2011.

9. Elekta, A new TMR dose algorithm in Leksell Gamma Plan, White Paper, Stockholm, Sweden 2012

10. Fippel M., Fast Monte Carlo dose calculation for photon beams based on the VMC electron algorithm. Medical physics, Vol. 26:1466-75., 1999

11. Jiang X, Yuan L, Engelbach JA, Cates J, Perez-Torres CJ, Gao F, et al. (2015) A Gamma-Knife-Enabled Mouse Model of Cerebral Single-Hemisphere Delayed Radiation Necrosis. PLoS ONE 10(10): e0139596. doi:10.1371/journal.pone.0139596

12. Jiang, X., MRI Characterization of Radiation Necrosis in an Animal Model: Time to Onset, Progression, and Therapeutic Response

13. Kazemi, K. et al, Design and construction of a brain phantom to simulate neonatal MR images Computerized Medical Imaging and Graphics 35 237-350, 2011

14. Lu W, Chen M, Mackie TR, Olivera GH and Reckwerdt PJ., Accurate convolution/superposition for multiresolution dose calculation using cumulative tabulated kernels. Physics in Medicine and Biology, Vol. 50:655-680,2005

15. Marcusm, GammaPlan Leksell Gamma Knife radiosurgery treatment planning verification method, Med Phys 2000

16. Moskvin, V.P., Henderson, M.A., Barriger, B., Cao M., DesRosiers C., Johnstone, P., Das I.J., Inhomogeneity Correction using Monte Carlo Simulation for Leksell Gamma Knife Stereotactic Radiosurgery, I.J. Rad Onc Bio Phys Vol 75(3), Supplement, p.S680, 2009

17. Moskvin, V., Timmerman, R., DesRosiers, C., Randall, M., DesRosiers, P., Dittmer, P., Papiez, L., Monte Carlo simulation of the Leksell Gamma Knife: II. Effects of heterogeneous versus homogeneous media for stereotactic radiosurgery, Phys. Med. Biol. 49 4879–4895, 2004

18. Nakamura JL, Comparison of intensity modulated radiosurgery with gamma knife radiosurgery for challenging skull base lesions, Int J Rad Onc Bio Phys, 2003

19. Nakazawa, H., Komori, M., Shibamoto, Y., Takahhiko, T., Yoshimasa, M., Tatsuya, K., Dosimetric comparison of absolute and relative dose distributions between tissue maximum ratio and convolution algorithms for acoustic neurinoma plans in Gamma Knife radiosurgery, Acta Neurochirurgica, V. 156, Issue 8, pp.1483-1489, 2014

20. Oshiro, Y., T. Aruga, K. Tsuboi, K. Marino, R. Hara, Y. Sanayama, J. Itami, Stereotactic Body Radiotherapy for Lung Tumors at the Pulmonary Hilum, I. J. Radiation Oncology Biology Physics Volume 75, Number 3, Supplement, 2009

21. Romano, F., Sabini, M.G., Cuttone, G., Russo, G., Mongelli, V., Foroni, R., Geant4-Based Monte Carlo Simulation of the Leksell Gamma Knife®, 2007 IEEE Nuclear Science Symposium Conference Record

22. Saff E and Kuijlaars A., Distributing many points on a sphere. The Mathematical Intelligencer, Vol. 19:5–11.,1997

23. Salvat F, Fernández-Varea JM and Sempau J., 2006 PENELOPE-2006: a code system for Monte Carlo simulation of electron and photon transport", NEA Report 6222 www.nea.fr/html/science/pubs/2006/nea6222-penelope.pdf, 2006

24. Sheparda, D.M., Inverse treatment planning for Gamma Knife radiosurgery, Med. Phys. 27 .12., December 2000

25. Shirikant S., Rockwell Mackie, T., et. al., Monte Carlo and Convolution Dosimetry for Stereotactic Radiosurgery, Int J Rad Onc Bio Phys, Vol. 19 pp. 1027-1035

26. Webster, G., Hardy, M., Rowbottom, C., Mackay, R., Design and implementation of a head-and-neck phantom for system audit and verification of intensity-modulated radiation therapy, J. Applied Clinical Med Phys, Vol 9 (2) 2008

27. Xiong, W., D. Huang, L. Lee, J. Feng, K. Morris, E. Calugaru, C. Burman, J. Li, C. Ma, Inhomogeneity Effect on Gamma Knife SRS, Proceedings of the 48th ASTRO Meeting

28. Xu, Andy, Jagdish Bhatnagar, Greg Bednarz, Ajay Niranjan, John Flickinger, L. Dade Lunsford, M. Saiful Huq , Dose differences between the three dose calculation algorithms in Leksell GammaPlan, J Appl Clin Med Phys. Sep 8;15(5):4844, 2014

29. Zhang P, Dean D, Fast verification of gamma knife treatment plans, J Appl Clin Med Phys 2000

VITA

After attending the University of Missouri for undergraduate studies, I joined the Nuclear Science and Engineering Institute to begin studying in Medical Physics. During my Master's degree program, I was able to do research with Dr. Jacqueline Esthappan in the Radiation Oncology department at Washington University in St. Louis. This lead to me being able to transition to doing research and attending class lectures in that same department while I pursued my PhD.

At the time of finishing my dissertation defense, I am a first year Medical Physics Resident at Northwestern Memorial Hospital in Chicago, Il.